Irrigation Science
https://doi.org/10.1007/s00271-022-00789-9

ORIGINAL PAPER

Application of the vineyard data assimilation (VIDA) system to vineyard root-zone soil moisture monitoring in the California Central Valley

Fan Chen[1,2] · Fangni Lei[3] · Kyle Knipper[4] · Feng Gao[1] · Lynn McKee[1] · Maria del Mar Alsina[5] · Joseph Alfieri[1] · Martha Anderson[1] · Nicolas Bambach[6] · Sebastian J. Castro[7,8] · Andrew J. McElrone[7,8] · Karrin Alstad[9] · Nick Dokoozlian[5] · Felix Greifender[10] · William Kustas[1] · Claudia Notarnicola[10] · Nurit Agam[11] · John H. Prueger[12] · Lawrence E. Hipps[13] · Wade T. Crow[1]

Received: 12 November 2021 / Accepted: 18 March 2022

Abstract
Efforts to apply gridded root-zone soil moisture (RZSM) products for irrigation decision-support in vineyards are currently hampered by the difficulty of obtaining RZSM products that meet required accuracy, resolution, and data latency requirements. In particular, the operational application of soil water balance modeling is complicated by the difficulty of obtaining accurate irrigation inputs and representing complex sub-surface water-flow processes within vineyards. Here, we discuss prospects for addressing these shortcomings using the Vineyard Data Assimilation (VIDA) system based on the assimilation of high-resolution (30-m) soil moisture information obtained from synthetic aperture radar and thermal-infrared (TIR) remote sensing into a one-dimensional soil water balance model. The VIDA system is tested retrospectively (2017–2020) for two vineyard sites in the California Central Valley that have been instrumented as part of the Grape Remote sensing Atmospheric Profile and Evapotranspiration eXperiment (GRAPEX). Results demonstrate that VIDA can generally capture daily temporal variations in RZSM for vertical depths of 30–60 cm beneath the vine row, and the assimilation of remote sensing products is shown to produce modest improvement in the temporal accuracy of VIDA RZSM estimates. However, results also reveal shortcomings in the ability of VIDA to correct biases in assumed irrigation applications—particularly during well-watered portions of the growing season when TIR-based evapotranspiration observations are not moisture limited and, therefore, decoupled from RZSM. Prospects for addressing these limitations and plans for the near-real-time operational application of the VIDA system are discussed.

✉ Fan Chen
fan.chen@usda.gov

1 USDA ARS Hydrology and Remote Sensing Laboratory, Beltsville, MD, USA

2 SSAI Inc., Lanham, MD, USA

3 Geosystems Research Institute, Mississippi State University, Starkville, MS, USA

4 USDA ARS Sustainable Water Systems Research Laboratory, Davis, CA, USA

5 Department of Winegrowing Research, E and J Gallo Winery, Modesto, CA, USA

6 Department of Land, Air and Water Resources, University of California, Davis, CA, USA

7 USDA-ARS, Crops Pathology and Genetics Research Unit, Davis, CA, USA

8 Department of Viticulture and Enology, University of California, Davis, CA, USA

9 Interagency Ecological Program, California Department of Fish and Wildlife, Stockton, CA, USA

10 Institute for Earth Observation, Eurac Research, 39100 Bolzano, Italy

11 French Associates Institute for Agriculture and Biotechnology of Drylands, Blaustein Institutes for Desert Research, Ben-Gurion University of the Negev, Midreshet Ben-Gurion, Israel

12 USDA-ARS, National Laboratory for Agriculture and the Environment, Ames, IA, USA

13 Plants, Soils and Climate Department, College of Agriculture and Applied Sciences, Utah State University, Logan, UT, USA

Published online: 23 April 2022

Introduction

Irrigated crops make a large and growing contribution to global agricultural production (Kukal and Irmak 2019). However, the expanding water-use footprint for irrigation is increasingly coming into conflict with competing water-resource users. Such conflict is particularly critical for growers of high-value fruit and nut crops that rely heavily on irrigation in water-limited areas like the Central Valley of California. Recent droughts in the western United States have led to the increased exploitation of groundwater resources within the Central Valley to offset large, and likely growing, inter-annual variability in surface water availability (due, e.g., to large year-to-year variations in winter snowfall within the Sierras Jasechko and Perrone 2020). In response, the Californian Sustainable Groundwater Management Act now mandates that planned irrigation activities be made consistent with the sustainable extraction of groundwater resources. Given that climate conditions in central and eastern California appear to be trending towards a prolonged (potentially multi-decadal) period of increased inter-annual variability (Diffenbaugh et al. 2015), perhaps superimposed on a concurrent drying trend (Huning and AghaKouchak 2018), significant advances in irrigation efficiency are needed to maintain the economic value of Central Valley fruit and nut crops while simultaneously ensuring the long-term sustainability of its groundwater resources.

At least in theory, such opportunities exist for California grape growers. Studies have consistently demonstrated that, if properly timed and calibrated, vineyard irrigation levels can be reduced below evapotranspiration rates (i.e., deficit irrigation) without incurring significant negative impacts on grape yield. In fact, the proper temporal allocation of modest water stress can, in many cases, improve the quality of grapes for wine production (Acevedo-Opazo et al. 2010; Zarrouka et al. 2012). Likewise, the increased utilization of variable rate drip irrigation (VRDI) systems in vineyards provides a means by which managers can utilize fine-resolution biophysical observations to spatially optimize irrigation (Sanchez et al. 2017).

However, excessive water stress can damage the carrying capacity of grapevines over multiple seasons and poses a serious risk for producers (Shellie 2014; Keller et al. 2016). Such risk places relatively stringent accuracy requirements on biophysical variables used to map the time/space evolution of vine water stress. Of these variables, root-zone soil moisture (RZSM) is particularly important. Plant-available soil water (PAW, the percentage level of RZSM above permanent wilting point and below field capacity) is an important indicator for timing the onset of irrigation in response to the drying of the soil column during the early growing season. Later in the growing season, continuous monitoring of RZSM helps ensure that irrigation meets crop water-use requirements (i.e., evapotranspiration, ET)–which enables managers to calibrate the application of water stress if necessary. Unfortunately, RZSM levels are notoriously difficult to track in a fine-resolution and spatially continuous manner and existing products currently do not meet accuracy requirements for the credible management of vineyard irrigation and water-stress levels (Lei et al. 2020).

When applied individually, all existing RZSM monitoring approaches suffer from serious limitations. For example, while strides have been made in the development of in situ soil moisture instrumentation, such observations typically reflect RZSM conditions within only a highly localized spatial domain (on the order of 10 cm^3). Upscaling such fine-scale observations into a spatially continuous analysis is challenging due to the very high level of unorganized, fine-scale RZSM variability typically present in an agricultural field (Hupet and Vanclooster 2002). VRDI adds an additional level of complexity to this issue by introducing structured RZSM spatial variability. These difficulties can be overcome through in situ measurement only via the use of extremely intensive (i.e., dense) and costly soil RZSM networks. As a result, the application of ground-based soil moisture sensors to operational irrigation scheduling has generally been confined only to a few limited testbed sites.

Likewise, advances have been made in the application of satellite remote sensing approaches to retrieve soil moisture (e.g., Oh 2004; Naeimi et al. 2009; Chan et al. 2018; Al Bitar et al. 2017; Das et al. 2019). Relative to ground-based observations, these approaches have obvious advantages with regard to their scalability over large spatial domains. However, the most accurate of these approaches, L-band passive microwave remote sensing, suffers from poor spatial resolution (generally > 10 km) and, therefore, remains incapable of resolving individual agricultural production units. Much finer resolution (< 100 m) is possible via the use of synthetic aperture radar (SAR) to process active microwave backscatter measurements (Attarzadeh et al. 2018; El Hajj et al. 2017; Gao et al. 2017). However, this improved resolution comes at a cost of increased sensitivity to surface roughness and vegetation structure and a decrease in the temporal frequency of retrievals. In addition, all microwave techniques, whether active or passive, are constrained by their shallow vertical penetration depth that limits them to the retrieval of only near-surface (0–5 cm) soil moisture (SSM) conditions.

An alternative remote-sensing strategy is the use of thermal-infrared (TIR) remote sensing to detect the onset and level of plant water stress via an increase in vine-canopy temperature (Gerhards et al. 2019). This approach has the large advantage of reflecting root-zone, as opposed to simply surface, soil moisture availability since the ability of the vine canopy to cool itself down to air temperature levels reflects, among other things, its capacity to extract water from the root-zone for transpiration. In this way, TIR surface temperature retrievals, and evapotranspiration (ET) estimates based on these retrievals, can be used as a proxy for RZSM (Hain et al. 2009). However, TIR approaches are limited only to clear-sky conditions. In addition, the role of important co-varying parameters (e.g., leaf area index and micrometeorological variables) must be properly accounted for when attempting to constrain RZSM using TIR-based ET retrievals (Crow et al. 2008).

A third, and final, potential source of RZSM information are spatially distributed and vertically discretized soil water balance models (e.g., Verdoodt et al. 2005; Crow et al. 2008; Noorduijn et al. 2018). These models attempt to predict the transport of rainfall or irrigation through the soil column using meteorological observations and water and energy balance considerations. They provide RZSM estimates that are continuous in both space and time and can be set-up to represent nearly any potential combination of discrete vertical soil layers. However, they are based on the implicit assumption that all key factors describing the temporal evolution of RZSM and ET are known and accurately represented by the model. Given the known complexity of sub-surface flow conditions in agricultural fields (Gish et al. 2005), this assumption is extremely optimistic in vineyards. In addition, water balance models require timely, accurate irrigation inputs to track RZSM and ET. Such information is almost never available over large geographic areas of individually operated units, which severely limits the application of soil water balance models within irrigated croplands.

Given the limitations of any individual RZSM monitoring approach, one promising path forward uses data assimilation techniques that combine *multiple* strategies for monitoring RZSM within a unified analysis. Data assimilation is a mathematical strategy for guiding a dynamic model (e.g., a soil water balance model) using incomplete and non-perfect observations (e.g., remotely sensed SSM and ET) that have a known relationship with, potentially unobserved, model states of interest (e.g., RZSM). Here, we describe the development and operational application of the Vineyard Data Assimilation (VIDA) system to track high-resolution (30-m) daily RZSM variations within California Central Valley vineyards. VIDA is based on the simultaneous assimilation of SAR-based SSM retrievals and TIR-based ET estimates into a soil water balance model using an Ensemble Kalman Filter (EnKF). In this way, VIDA attempts to address deficiencies in bottom-up water balance modelling using (uncertain and incomplete) top-down remote sensing retrievals of SSM and ET.

This paper will describe the VIDA system and its recent application within several California vineyards instrumented as part of the Grape Remote sensing Atmospheric Profile and Evapotranspiration eXperiment (GRAPEX; Kustas et al. 2018). In particular, we will discuss prospects for meeting RZSM product requirements for vineyard irrigation management using a combination of soil–water balance modelling and current (and planned) satellite remote sensing sources. We will also highlight remaining data assimilation challenges affecting the VIDA RZSM analysis.

Vineyard data assimilation (VIDA) system

The VIDA system consists of the following two parts: a soil water balance model ("WEB-SVAT") and an EnKF procedure for correcting soil–water balance errors via the assimilation of TIR-based ET and SAR-based SSM retrievals ("Ensemble kalman filtering").

WEB-SVAT

Soil water balance modelling in VIDA is based on the hourly, 30-m application of the Water-Energy-Balance Soil–Vegetation–Atmosphere-Transfer (WEB-SVAT) model created by merging the modified two-source energy balance (TSEB) scheme of (Norman et al. 1995); see "WEB-SVAT energy balance" with the simplified force-restore approach to the soil water balance introduced by (Noilhan and Planton 1989) and later adapted by both (Montaldo et al. 2001; Crow et al. 2008) ("WEB-SVAT soil–water balance"). Given the importance of seasonality on vineyard water balance considerations, "Vineyard phenological stages" outlines our approach for representing discrete phenological stages in seasonal vine and interrow cover-crop development.

Due to the clumped nature of the vineyard vegetation canopy, as well as its concentrated root system underneath the vine-row, a two-tile (i.e., vine-row and interrow) spatial surface geometry is adopted (see Fig. 1). Note that individual vine-rows are not explicitly resolved by our 30-m application resolution. Therefore, the WEB-SVET model is designed to conceptually represent sub-grid vine-row and interrow tiles. This row/interrow tile approach allows for a detailed representation of vineyard vegetation dynamics due to both seasonal growth stages (e.g., budbreak, flowering, and veraison) and management activities (e.g., cover-crop seeding and removal, vine pruning, and harvest).

WEB-SVAT energy balance

Energy balance estimates generated by WEB-SVAT are based on the application of the TSEB canopy model to estimate a single pair of canopy transpiration and soil evaporation flux estimates within each 30-m WEB-SVAT pixel. These (pixel-scale) flux estimates are then extracted

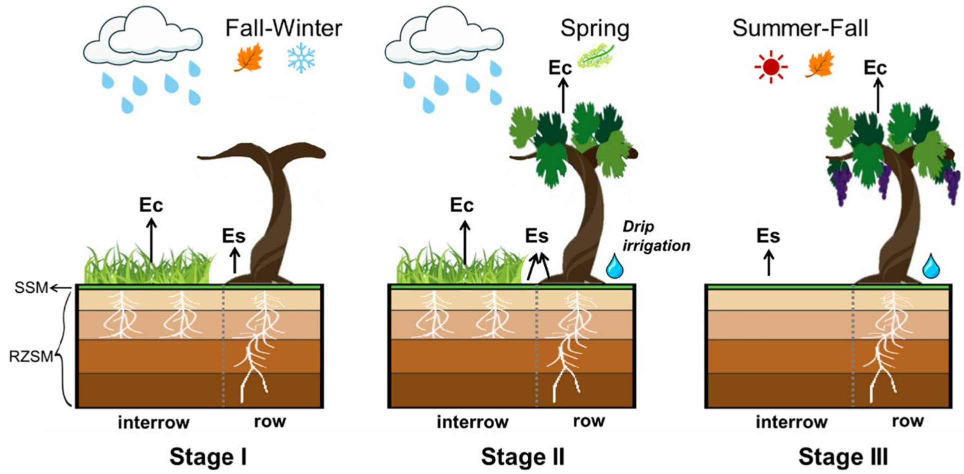

Fig. 1 Conceptual representation of the three phenological stages in the VIDA two-tile system of vegetation dynamics in a vineyard. ES and EC represent soil evaporation and canopy transpiration; SSM and RZSM represent surface and rootzone soil moisture, respectively. See "Vineyard phenological stages" for a detailed description of each stage

from soil moisture states within (sub-pixel) vine-row and interrow tiles using assumptions presented in "Vineyard phenological stages" and illustrated in Fig. 1. Note that the TSEB formulation presented here contrasts with the classical TSEB application (see, e.g., Norman et al. 1995) in that surface temperatures are *internally* calculated by the WEB-SVAT via energy balance considerations—as opposed to *externally* observed using TIR remote sensing. Nevertheless, the assumed structure/geometry of the TSEB model is not altered.

The TSEB vegetation canopy model partitions energy fluxes between soil and vegetation via separate energy balance equations as follows:

$$\begin{array}{l} R_N = R_{N,C} + R_{N,S} \\ R_{N,C} = H_C + LE_C \\ R_{N,S} = H_S + LE_S + G \end{array}, \tag{1}$$

where H and LE are sensible and latent heat fluxes, and subscripts "$_S$" and "$_C$" denote the soil and canopy, respectively. Net radiation (R_N) received by the canopy ($R_{N,C}$) and soil ($R_{N,S}$) is calculated based on the radiative transfer model of (Campbell and Norman 1998) using observations of downward solar radiation (S) and above-canopy downward longwave radiation ($L_\downarrow$) as follows:

$$\begin{array}{l} R_{N,C} = \left(1-\tau_{lw}\right)\left(L_\downarrow + \varepsilon_S\sigma T_S^4 - 2\varepsilon_C\sigma T_C^4\right) + \left(1-\tau_{Sw}\right)\left(1-\alpha_C\right)\cdot S \\ R_{N,S} = \tau_{lw}L_\downarrow + \left(1-\tau_{lw}\right)\varepsilon_C\sigma T_C^4 - \varepsilon_S\sigma T_S^4 - \varepsilon_S\sigma_C^4 + \tau_{lw}\left(1-\alpha_S\right)\cdot S, \end{array} \tag{2}$$

where ε, α, and T are the emissivity, albedo, and temperature of soil and canopy, respectively, σ the Stephen–Boltzman constant, and τ the canopy transmissivity for both shortwave (subscript "*sw*") and longwave ("*lw*") radiation. Ground heat flux G is calculated as a fraction of $R_{N,S}$ that varies as a function of time of day using a double asymmetric sigmoid function (Nieto et al. 2019).

Following (Hashemian et al. 2015), the parallel version of the TSEB canopy model is adopted for sensible heat and latent heat calculations as follows:

$$\begin{array}{l} H_C = \rho_{air}C_P\left(T_C - T_A\right)/R_A \\ H_S = \rho C_P\left(T_S - T_A\right)/\left(R_A + R_{A,S}\right) \end{array}, \tag{3}$$

where ρ_{air} is air density, and C_P is the specific heat of air at constant pressure. R_A is the above-canopy aerodynamic resistance, and $R_{A,S}$ the within-canopy soil aerodynamic resistance.

Potential latent heat flux from the canopy ($LE_{C,max}$) is then estimated by the Penman–Monteith equation:

$$LE_{C,max} = \frac{\left(\Delta R_{N,C} + \frac{\rho_{air}C_P\left[e_S(T_C)-e_a\right]}{R_A}\right)}{\Delta + \gamma\left(1 + \frac{R_C}{R_A}\right)}, \tag{4}$$

where γ is the slope of the saturation vapor pressure versus temperature curve; $e_S\left(T_C\right)$ is the saturated vapor pressure at average canopy height; e_a is the observed above canopy vapor pressure; and R_C is the canopy resistance to vapor transfer.

To estimate actual canopy transpiration, $LE_{C,max}$ estimates acquired from (4) are combined with the f_{PET} parameter derived from soil water availability and root density distribution considerations (see "WEB-SVAT soil–water balance"). In particular, f_{PET} is applied in the TSEB iteration to estimate the fraction of $LE_{C,max}$ to be extracted from each rootzone layer (except the top 0–5 cm layer) to determine the total actual canopy transpiration:

$$LE_C = \sum_{i=2}^{n} (f_{PET\_R,i} + f_{PET\_IR,i}) \cdot LE_{C,max}, \quad (5)$$

where $f_{PET\_R,i}$ and $f_{PET\_IR,i}$ are the fraction of $LE_{C,max}$ to be extracted from the *i*th soil layer of the vine-row and interrow, respectively. Latent heat flux due to direct soil evaporation is then calculated as follows:

$$LE_S = \rho C_p \gamma^{-1} \left[\frac{e_s(T_S) - e_a}{R_{A,S} + R_A + R_S} \right], \quad (6)$$

where R_S is the soil resistance to surface evaporation calculated following (Sellers et al. 1992). Dividing LE_C and LE_S by the latent heat of vaporization converts them into equivalent (water depth per time) estimates of E_C and E_S, respectively, that are required for WEB-SVAT soil water balance calculations described below in "WEB-SVAT soil–water balance".

At each hourly WEB-SVAT time step, model estimates of T_C and T_S are derived using an iterative root-finder that converges to temperature estimates that simultaneously respect all constraints in (1–6). For the first time step in a simulation, T_C and T_S are initialized to match observed 2-m air temperature. The process is terminated when a maximum iteration number is reached; a warning is generated and T_C and T_S values from the last iteration are used in subsequent calculation. The Newton–Raphson method employed ensures that in such rare instances, the solutions achieved are a better approximation to the true values of T_C and T_S under given conditions than the over-simplified initial guess and, therefore, accepted instead of being discarded.

Vineyard phenological stages

As noted above, the WEB-SVAT water balance is solved separately for sub-pixel vine-row and interrow tiles. Due to strong seasonality in the water balance for these tiles, we divide the annual cycle of a typical vineyard into three general stages (see Fig. 1).

Stage I is characterized by grass-only vegetative cover between the start of vine-leaf senescence (October/November) until budbreak during the following spring (March/April). As such, it is assumed to begin when autumn Normalized Difference Vegetation Index (NDVI) values fall below 0.33 (or October 1, whichever comes first) and ends on March 31 of the following year. During this stage, only the interrow grass is assumed to be actively transpiring, and the vine-row is treated as bare soil that provides the sole source for E_S. Cover-crop roots are concentrated (~90%) in the upper 90 cm and assumed to grow slowly deeper (e.g., root fraction between 30 and 60 cm increases from ~10 to 25%) from the beginning of Stage I until April 1—at which point they are assumed to be static until the end of Stage II (see below).

Stage II is characterized by concurrent grass and vine-canopy cover. It begins with vine-leaf emergence (March/April) and ends in early summer (June) when the interrow cover crop is normally mowed or dry. For vineyards located in the California Central Valley, Stage II is assumed to run between April 1 and May 31. During this period, the vine-row and interrow contribute to both E_C and E_S. Therefore, both water flux types are simultaneously extracted from all sub-pixel tiles. During Stage II, vine roots grow progressively deeper (e.g., root fraction below 90 cm increases from ~25 to 45%) and reach a final static distribution that remains constant throughout Stage III.

Stage III is characterized by vine-only vegetation cover and runs from early summer through harvest. The stage is assumed to begin on June 1 and lasts until the NDVI condition for the onset of Stage I is met (see above). During Stage III, the interrow cover crop is assumed to be removed or senescent—leaving only non-transpiring stubble or bare soil in the interrow. Due to a lack of summer rainfall in the California Central Valley, soil water recharge (via irrigation) as well as canopy transpiration is generally limited to the vine-row during this stage. Hence, E_C is extracted solely from the vine-row and E_S solely from the interrow.

WEB-SVAT soil–water balance

E_S and E_C estimates obtained from (5) to (6) are combined with rainfall and/or irrigation inputs to solve the multi-layer soil water balance equations following (Lei et al. 2020). The soil water profiles of the vine-row and interrow are calculated separately based on the vertical discretization of the soil column into five layers: 0–5 cm, 5–30 cm, 30–60 cm, 60–90 cm, and below 90 cm. The thickness of the deepest layer depends on the soil profile depth obtained from the SSURGO (Soil Survey Geographic Database) dataset.

While rainfall is uniformly applied to both sub-pixel tiles, irrigation is received only by the vine-row tile (see Fig. 1). In addition to the (horizontal) vine-row/interrow separation described above in "Vineyard phenological stages", sources for E_S and E_C are also separated along the soil vertical profile. In particular, E_S is extracted only from the surface layer (0–5 cm) while E_C is extracted throughout the soil profile according to the assumed vertical distribution of vine and cover-crop roots.

As mentioned in "WEB-SVAT energy balance", the energy and soil water balance components of WEB-SVAT are linked by the f_{PET} parameter, which represents the estimated fraction of potential transpiration that can be extracted from rootzone soil layers. Given estimated levels of soil water in each vertical soil layer, as well as the fraction of root density in each rootzone soil layer, f_{PET} is calculated via an exponential root-water uptake model (see Li et al. 2001; Lei et al. 2020). In addition to evaporative fluxes, WEB-SVAT also captures inter-layer diffusive and drainage water fluxes using the approach described in (Hashemian et al. 2015).

Ensemble kalman filtering

WEB-SVAT RZSM estimates are degraded by a range of error sources–most notably our ignorance of true irrigation inputs, sub-surface water flow patterns, and spatial variations in crop water loss. VIDA attempts to mitigate these errors through the assimilation of remotely sensed SSM and ET products into WEB-SVAT. The Ensemble Kalman Filter (EnKF) is a widely used sequential data assimilation technique that integrates discrete observations with continuous model background estimates. The relative weighting factor (i.e., Kalman gain) applied to the assimilated observations is determined by comparing estimates of observation error covariance with model forecast error covariances sampled from a Monte-Carlo ensemble of model replicates—generated by applying random synthetic perturbations to WEB-SVAT states, forcing data, and parameters.

Using a 25-member EnKF, 30-m TIR-based ET and 20-m SAR-based SSM products are simultaneously assimilated into WEB-SVAT to update (multi-layer) model estimates of both vine-row and interrow soil moisture. See "Study area and data" below for a complete description of these remote sensing products. The background WEB-SVAT forecast ensemble is generated via multiplicative perturbations applied to precipitation and irrigation forcing estimates— along with additive perturbations applied to LAI, air temperature, and incoming solar radiation inputs. The EnKF control vector, representing the WEB-SVAT model states updated by the EnKF, consists of volumetric soil moisture (VSM) estimates for all ten vine-row and interrow soil layers (i.e., five soil layers in each tile). See (Lei et al. 2020) for further details on the implementation of the EnKF within VIDA.

Study area and data

Study area

This study was conducted primarily in three vineyard blocks managed by E&J Gallo Winery within the California Central Valley. Two adjacent blocks of interest (SLM001 and SLM002) are located near Lodi, CA (Fig. 2). Soils in SLM001 and SLM002 are predominantly Kimball silt loam with 0–8 percent slope. SLM001 contains 364 Landsat 30-m pixels (26 rows and 14 columns) and SLM002 224 pixels (16 rows and 14 columns). Pinot Noir (*Vitis vinifera L.*) was planted in 2009 for SLM001 and 2011 for SLM002. However, in early 2020, SLM001 was re-grafted to Cabernet Sauvignon and SLM002 to Merlot (*Vitis vinifera L.*). Both SLM001 and SLM002 are equipped with a drip irrigation system that has a designed application rate of 4 L per hour per vine.

The RIP720 block located near Fresno, CA was planted with Merlot in 2010 and contains 156 Landsat 30-m pixels (12 rows by 13 columns). Soil texture is loam/sandy loam with 0–1 percent slope. RIP720 is equipped with a VRDI system capable of separately irrigating each of its 156 30-m sub-blocks with a designed application rate of 3 L per hour

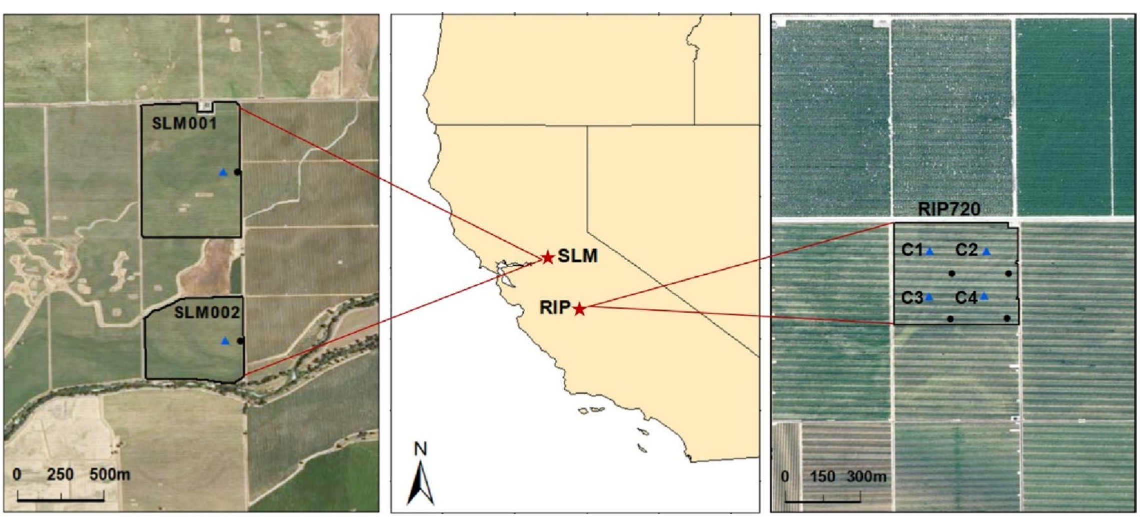

Fig. 2 Location of the SLM and RIP720 vineyard blocks. Profile soil moisture sampling sites are shown as blue triangles and eddy covariance flux towers as black circles. Transect surface soil moisture sampling sites within SLM001 and SLM002 are collocated with shown flux towers

per vine. Specific irrigation amounts in each sub-block are achieved by controlling the duration of application.

Vines in SLM001, SLM002, and RIP720 are all trained on a split trellis with 1.52-m vine spacing and 3.35-m row width and an east–west row orientation. As part of the GRAPEX project, extensive monitoring of the micrometeorological, surface energy balance and profile VSM variables have been conducted since 2013 at the SLM blocks and 2018 at RIP720. Detailed block and instrumentation descriptions can be found in (Kustas et al. 2018; Knipper et al. 2019b; Wilson et al. 2020; and Semmens et al. 2016). The SLM and RIP blocks are each located within a larger (100 km^2) domain where VIDA was test-run operationally during the 2021 growing season (see "Overview of operational application").

Ground measurements

For validation purposes, special emphasis is placed on eight Landsat 30-m pixels in the SLM001, SLM002, and RIP720 vineyard blocks containing extensive GRAPEX ground-based soil moisture instrumentation (Fig. 2).

The SLM001 and SLM002 profile VSM measurements consist of three sets of soil moisture profile sensors (HydraProbe, Stevens Water Monitoring System, Portland, OR) monitoring 30-, 60-, and -cm depths under the vine-row. Nearby (i.e., within 40 m), a SSM transect consisting of five equal-distance sensors at 5-cm depth is deployed across a vine-row and interrow, with two sensors in the vine-row and three sensors in the interrow. Averages obtained across this transect are considered comparable to the areal-mean SSM obtained from a – 30-m remote-sensing footprint. The SSM transects in the SLM blocks are part of a larger SSM sensor array used in a previous soil heat flux study; see (Agam et al. 2019) for complete description of the sensor layout. Approximately 50 m to the east of each profile soil moisture site at SLM, an eddy covariance tower has been collecting micrometeorological and surface flux measurements since April 2013 (Alfieri et al. 2019). A second five-sensor SSM transect is installed immediately adjacent to each flux tower site. ET and other surface energy balance components are derived from post-processing of the eddy covariance measurements (Alfieri et al. 2019). Given that surface winds are predominately from the west, and an assumed flux-tower footprint of – 100 m in the upwind direction (Li et al. 2008), ET estimates obtained at the flux tower site are assumed to be representative of the soil moisture profile pixels.

The RIP720 vineyard block has been divided into four quadrants with SSM transect (HydraProbe, see above) and profile soil moisture sensors (CS655 TDR probes, Campbell Scientific Inc., Logan, UT) located near the center of each quadrant, i.e., the C1, C2, C3, and C4 pixels labelled in Fig. 2. In each pixel, a VSM sensor array is deployed symmetrically from the center line of a vine-row to characterize both vertical and horizontal variability in the row and interrow. Interrow sensors monitor 5- and 30- cm depths at 75-cm distance from the centerline, and 5-, 40-, 60- and 90-cm depths at 165-cm distance. Vine-row sensors monitor 5-, 30-, 60, and 90-cm depths at 15-cm distance and 5-, 30-, and 60-cm depths at 45-cm distance. Each quadrant of RIP720 is also equipped with an eddy covariance flux tower located at its southeast corner (approximately 100 m from the quadrant center) since April 2018. Given the dominant northwest wind direction for the block, surface flux observations at these towers are considered representative of the C1–4 pixels.

Meteorological forcing, irrigation inputs, and soil parameters

Hourly meteorological forcing data (i.e., solar radiation, air temperature, wind speed, precipitation, and relative humidity) required for WEB-SVAT are obtained from nearby California Irrigation Management Information System (CIMIS) weather stations. Specifically, CIMIS #131 (Fair Oaks) observations are used for both SLM blocks and CIMIS #80 (Fresno State) for RIP720. Surface atmospheric pressure is obtained from the North American Land Data Assimilation System (NLDAS-2) L4 hourly 0.125° primary forcing data set (Xia et al. 2012).

Naturally, grape growers use different irrigation systems and scheduling strategies deemed suitable for, among other factors, the particular soil, grape cultivar, vine age, desired wine quality, and yield targets for individual blocks. Such decisions are commonly made weekly during the growing season based on the monitoring of meteorological trends and vine condition. Except for a small number of study sites, both historical irrigation records and real-time irrigation information are generally unavailable for the purpose of soil water balance modelling. Therefore, multiple realizations of synthetically generated irrigation inputs are used to force the WEB-SVAT model during the vine-growing season and generate a Monte-Carlo ensemble of VSM states reflecting uncertainty in irrigation inputs (see "Ensemble kalman filtering"). Specifically, a synthetic irrigation schedule for the SLM blocks was generated to match the average frequency and total amount of irrigation applied during the 2017–2020 growing seasons there on a monthly basis (between April and September) with an hourly application rate of 4 L/vine and converted into water depth estimates using an assumed wetting area of 1.2 m × 1.52 m. Given the lack of multi-year irrigation records for RIP720, synthetic irrigation is instead generated based on estimated growing-season crop water use of grape vines derived from average daily growing-season reference ET values from 2011 to 2020 obtained from nearby CIMIS stations, with a 3 L/vine hourly rate applied to the same wetting area as for the SLM blocks. As noted above, irrigation is received only by the WEB-SVAT vine-row tile.

Soil texture data are obtained from the online Web Soil Survey service (http://websoilsurvey.sc.egov.usda.gov/) provided by the USDA Natural Resources Conservation Service. Hydraulic parameters applied in power curves, describing the relationship between VSM, saturation hydraulic conductivity, and soil–water matric potential (see Lei et al. 2020, Appendix B) for each soil texture, are based on lookup tables provided by (Clapp and Hornberger 1978).

Daily LAI and NDVI time-series

Leaf area index (LAI) data products at 30-m resolution, required by both WEB-SVAT and TIR-based ET retrievals, are generated using Harmonized Landsat and Sentinel-2 (HLS) surface reflectance (SR) products (version 1.4, 3–4-day, 30-m) (Claverie et al. 2018), the Moderate Resolution Imaging Spectroradiometer (MODIS) LAI products (Collection 6, MCD15A3H, 4-day, 500-m) (Myneni et al. 2002; Yan et al. 2016) and LAI field measurements for three GRAPEX sites from 2013 to 2019 (White et al. 2019). A reference-based approach is used to build regression trees between LAI and SR using samples from two spatial resolutions (30-m and 500-m). The 500-m LAI-SR samples are produced from homogeneous MODIS pixels and the aggregated HLS SR product (Gao et al. 2012a; Sun et al. 2017). The 30-m LAI-SR samples are built on the field LAI measurements and 30-m HLS SR. The 500-m samples include general land cover types, while the 30-m samples focus specifically on vineyards. This combination of LAI retrievals provides complementary spatial and temporal information, and together can be used to produce 30-m LAI fields consistent with both MODIS LAI and field measurements (Gao et al. 2013). Once LAI and NDVI fields at Landsat-8 and Sentinel-2 overpass dates are generated, the smoothing and gap-filling processes described in (Gao et al. 2020) are applied to produce daily LAI and NDVI fields.

Assimilated satellite ET and SSM retrievals

As discussed above, the VIDA system simultaneously assimilates ET and SSM data products derived from satellite observations into the WEB-SVAT model. Here we describe these two data products in detail.

ALEXI/DisALEXI evapotranspiration

High-resolution (30-m) ET estimates are generated using the Atmosphere-Land Exchange Inverse (ALEXI) surface energy balance model (Anderson et al. 1997) and associated spatial disaggregation algorithm (DisALEXI; Norman et al. 2003; Anderson et al. 2004). The Two-Source Energy Balance (TSEB) model (see "WEB-SVAT" above) provides the conceptual foundation for ALEXI and DisALEXI by describing the land-surface exchange process for both soil and canopy components. ALEXI works by applying TSEB at two times during the morning period (– 1 h after sunrise and – 1 h before local noon) to estimate the time-integrated sensible heat influx into the atmospheric boundary layer, with surface temperature inputs (land surface temperature; LST) acquired via geostationary satellites. Daily latent heat flux is derived using the second LST retrieval (local noon) and the ratio of instantaneous to daily insolation following (Cammalleri et al. 2014). Due to its reliance on high temporal frequency LST imagery, ALEXI is typically constrained to the coarse spatial resolution of geostationary satellites (here 4-km). To map flux distributions at higher spatial resolution we utilize DisALEXI, which consists of executing TSEB over a gridded domain using LST retrievals obtained from Landsat (30-m, spatially sharpened following Gao et al. 2012b). The resulting DisALEXI ET maps are subsequently assimilated into VIDA with an assumed (one-sigma) observation error of 0.9 mm day^{-1} on days containing successful Landsat overpasses. This value is based on ET validation studies using flux tower observations acquired in Central Valley vineyards sites (Knipper et al. 2020).

Sentinel-1 surface soil moisture

Remotely sensed surface soil moisture (SSM) retrievals are derived from C-band (5.405 GHz) SAR instruments onboard the European Space Agency's Sentinel-1A and 1B satellites. The two-satellite constellation provides a theoretical revisit frequency of 6 days with an ascending node at 6:00 pm local solar time. The interferometric wide swath mode of Sentinel-1 maps radar backscatter at 5 m × 20 m resolution on 240-km swaths. The retrieval algorithm derives SSM at a 20-m ground resolution using a machine learning approach (Greifeneder et al. 2021).

Resulting SSM maps are resampled to the 30-m Landsat Worldwide Reference System (WRS) grid (UTM zone 10 N) via drop-in-bucket averaging and then, following established SSM data assimilation procedure, linearly rescaled to match the first (mean) and second (variance) statistical moments of the (pre-assimilation) WEB-SVAT SSM time-series for each 30-m pixel. Given differences in the incidence angle along the morning and afternoon Sentinel-1A and 1B tracks, the 6 am and 6 pm SSM retrievals are rescaled separately and then merged for VIDA assimilation. Assimilation is based on an assumed SSM retrieval error (one-sigma) of 0.04 m^3m^{-3} based on comparisons with ground-based SSM observations.

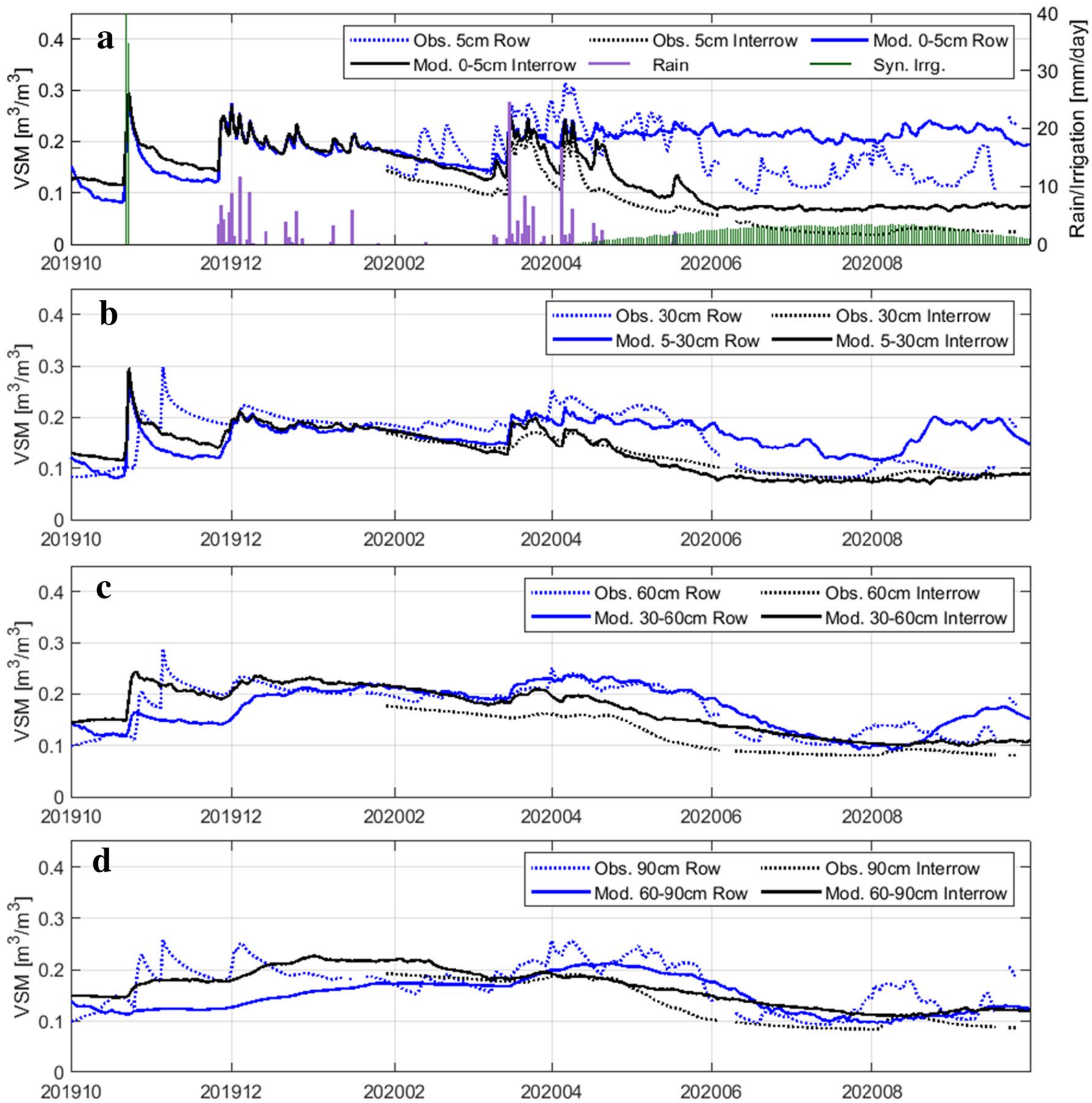

Fig. 3 Observed ("Obs.") and WEB-SVAT pre-assimilation ("Mod.") daily average VSM at the RIP720 C1 sampling site between October 1, 2019 and September 30, 2020 for four soil depths/layers. Observed VSM represents the depth indicated, while modelled VSM represents the layer average between the two depths given. Rainfall and synthetic irrigation are shown as purple and green bars in part a, respectively

Results and discussion

Pre-assimilation WEB-SVAT vine-row and interrow soil moisture estimates

Example pre-assimilation WEB-SVAT modelled vine-row and interrow VSM estimates obtained at the RIP720 site are shown in Fig. 3 alongside in situ measurements for the period October 1, 2019–September 30, 2020. Missing VSM observations in the interrow and vine-row between October 2019 and January 2020 are due to the removal of post-harvest soil moisture sensors during the fall of 2019. This removal is necessary since the interrow is disked and re-seeded with a cover crop yearly. Although the RIP720 block is equipped with a VRDI system, the same synthetic irrigation schedule, including a post-harvest flooding event, is applied to each pixel. The flooding event results in peak VSM levels across vine-row and interrow at the same time in late October each year, thus resetting the soil profile to a fully recharged state.

Between December and March, ground measurements indicate generally homogeneous vine-row and interrow VSM values responding to winter-precipitation events. However, multi-layer VSM levels in the row versus the interrow diverge in early February due to the start of vine-row (only) irrigation. The vigorous application of irrigation to support new vine growth in the spring (i.e., mid-April to mid-May) maintains high VSM in the vine-row while the interrow gradually dries once wintertime precipitation ends. The 5-cm soil moisture sensors in the vine-row respond rapidly to irrigation and remain the wettest (across all soil layers) throughout the growing season (Fig. 3a). The 30-, 60-, and 90-cm in situ sensors (in Fig. 3b–d, respectively) show a dampened, but comparable, level of response to irrigation—indicating good soil permeability and applied water reaching (at least) a depth of 90 cm.

Although pre-assimilation WEB-SVAT model results capture observed VSM temporal variability reasonably well, notable differences do occur. For example, the timing of irrigation onset represents a major source of uncertainty for the modelling of growing-season RZSM in vineyards. As described in "Meteorological forcing, irrigation inputs, and soil parameters", VIDA currently uses a simplified approach to synthetically represent irrigation that neglects inter-annual variability. The impact of this simplification is seen in modeled VSM during the 2020 growing season, when observed vine-row SSM peaks in February and early March (dotted blue lines, Fig. 3a). The timing of this peak suggests that irrigation began relatively early in the 2020 growing season to compensate for reduced wintertime precipitation. In contrast, synthetic irrigation inputs for WEB-SVAT do not start until April, leading to dry springtime biases in the modelled vine-row soil profile (see Fig. 3a–d). Further discussion of intra-seasonal irrigation variations will be presented in "Discussion and conclusions".

Table 1 Temporal correlation between observed SSM and pre-assimilation WEB-SVAT or Sentinel-1-retrieved SSM at four separate 30-m SLM pixels containing in situ SSM transects

	March–may		June–september	
	WEB-SVAT	Sentinel-1	WEB-SVAT	Sentinel-1
SLM001 profile	***0.937***	***0.838***	***0.259***	***0.672***
SLM001 transect	***0.910***	***0.862***	***0.360***	0.304
SLM002 profile	***0.811***	***0.830***	***0.180***	0.184
SLM002 transect	***0.849***	***0.843***	***0.222***	***– 0.557***

Bold and italicized values indicate corresponding p values below a 0.05 significance level

Another notable discrepancy is the inability of pre-assimilation WEB-SVAT to accurately capture observed dry-downs in the surface soil layer (see Fig. 3a) during the early summer. This is likely due to the neglect of soil evaporation from the vine-row tile in the vine-only growth stage (i.e., Stage III). WEB-SVAT estimates of temporal variations in deeper soil layers (see Fig. 3c, d) are relatively more accurate.

Similar seasonal patterns of vineyard vine-row and interrow SSM are observed at the SLM001 transect site in Fig. 4. Note that interrow profile VSM is not monitored at SLM. However, unlike RIP720 results in Fig. 3, significant (horizontal) irrigation seepage into the interrow is observed (see Fig. 4, between July and September 2018). This feature is missing in the modelled interrow time-series since WEB-SVAT assumes that applied water is restricted to the vine-row and neglects horizontal flows between vine-row and inter-row tiles. As a result, pre-assimilation WEB-SVAT results appear to over-estimate row versus interrow SSM differences.

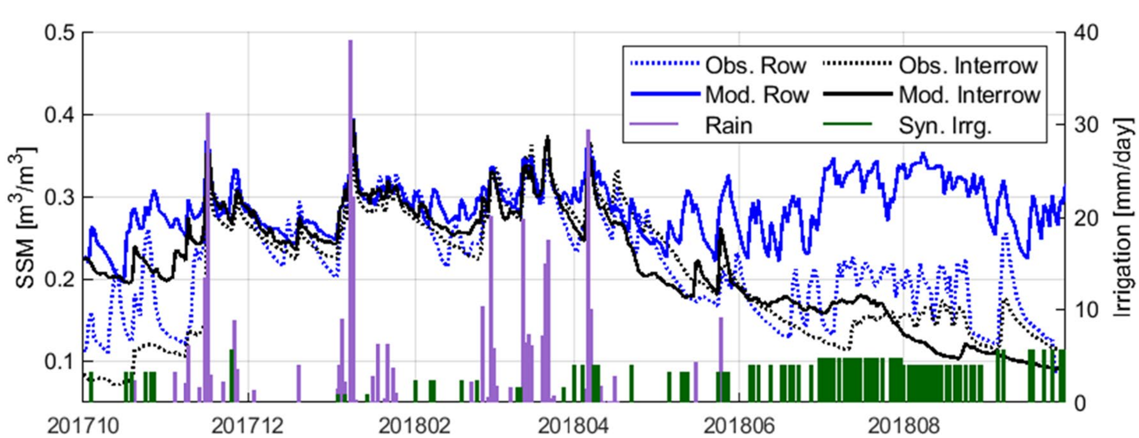

Fig. 4 Same as Fig. 3 except for only SSM (i.e., 0–5 cm) results at the SLM001 transect site

Remote sensing retrieval skill

Our stated goal of improving pre-assimilation WEB-SVAT RZSM estimates (see Figs. 3, 4 above) via the assimilation of satellite SSM and ET retrievals hinges on the ability of available satellite products to detect temporal errors in pre-assimilation WEB-SVAT soil moisture estimates. Here, we evaluate this potential separately for both Sentinel-1 SSM and DisALEXI ET retrievals.

Sentinel-1 SSM

Table 1 compares pre-assimilation WEB-SVAT and Sentinel-1 SSM time-series values with the transect average of SSM across the vine-row and interrow for four separate 30-m SLM pixels. Both WEB-SVAT and Sentinel-1 SSM estimates perform relatively well during the spring but degrade significantly during the summer. As discussed above, irrigation uncertainty is primarily responsible for poor WEB-SVAT SSM performance during the summer. On the other hand, degraded Sentinel-1 SSM skill in the summer likely reflects the attenuation of the soil backscattering signal caused by denser vine-canopy cover.

However, Sentinel-1 does not generally exhibit better temporal SSM skill than pre-assimilation WEB-SVAT results—even during the springtime when the vine canopy has not yet fully developed. However, Sentinel-1 also does not completely lose skill during the summer. For example, relatively good summer (i.e., June–September) correlation is found in the SLM001 profile pixel where WEB-SVAT performs relatively poorly (Table 1). In contrast, relatively lower Sentinel-1 correlation in the SLM002 block is likely associated with higher local LAI values found there.

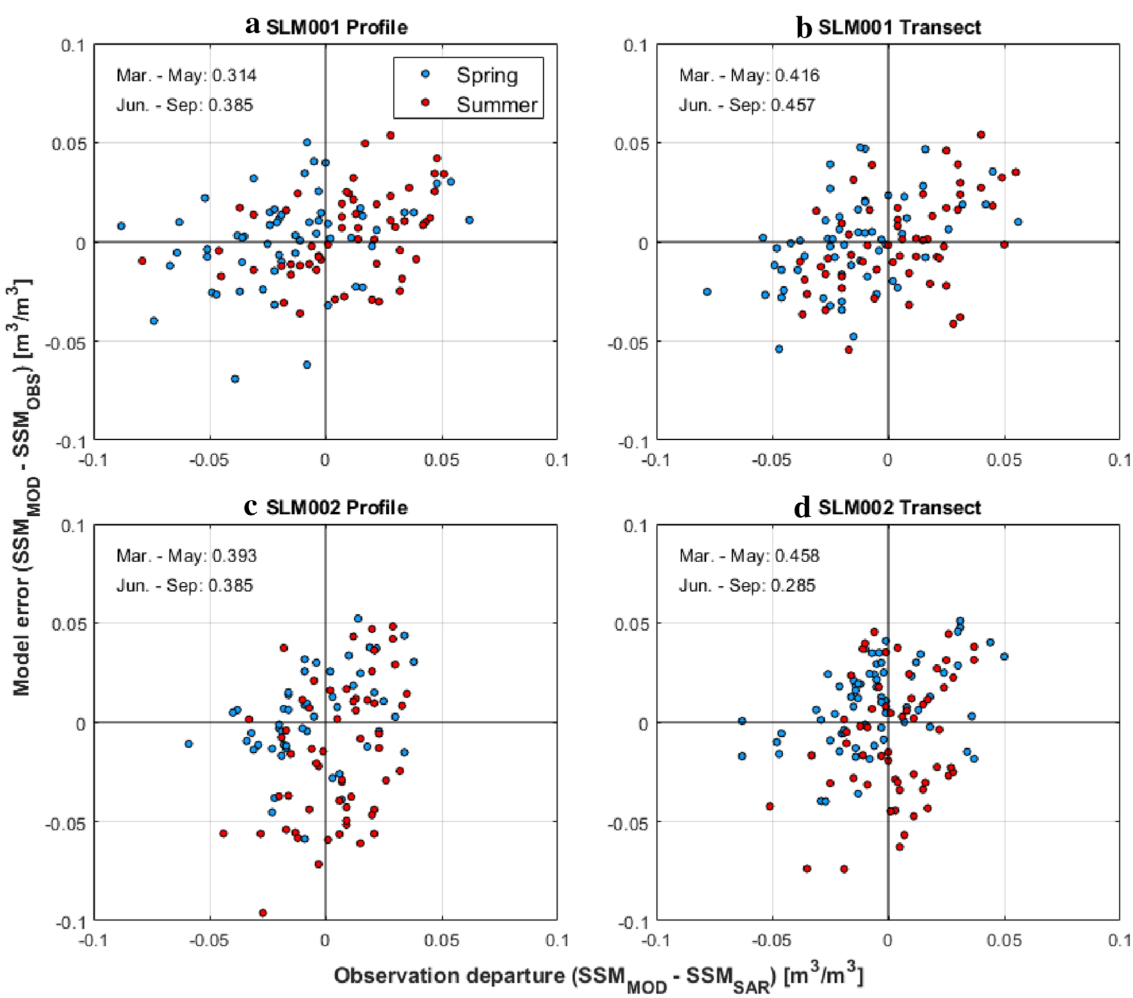

Fig. 5 Model pre-assimilation error in SSM (SSMMOD—SSMOBS) versus the departure between model pre-assimilation SSM and Sentinel SSM (SSMMOD—SSMSAR) at four instrumented pixels within the SLM001 and SLM002 blocks between January 01, 2017 and June 30, 2019. Data points are distinguished by season (spring: March–May, summer: June–September), and the sampled correlation between model error and observation departures is shown in the upper left of each subplot

Given the relatively good background skill of WEB-SVAT SSM estimates at the SLM001 and SLM002 sites in the early growing season, it is important to assess the marginal value of assimilating SSM retrievals there. For example, the additive skill of Sentinel-1 SSM retrievals for improving modelled SSM can be expressed by comparing model background error (i.e., pre-assimilation WEB-SVAT SSM minus in situ SSM) to model departures from satellite observations (i.e., pre-assimilation WEB-SVAT SSM minus Sentinel-1 SSM) (Fig. 5). When both observation departures and modelling errors have the same sign, sequential data assimilation increments will generally update soil moisture estimates in the correct direction and, therefore, improve the overall skill of SSM estimates. Paralleling the future treatment of Sentinel-1 SSM in "Sentinel-1 surface soil moisture" in VIDA, in situ SSM data in Fig. 5 are linearly scaled to match pre-assimilation WEB-SVAT SSM statistics prior to the calculation of displayed modelling errors. Results in Fig. 5 demonstrate that pre-assimilation WEB-SVAT error and remote sensing observation departures tend to be positively correlated and (generally) possess the same sign. Therefore, the assimilation of Sentinel-1 SSM retrievals can reasonably be expected to improve upon pre-assimilation WEB-SVAT SSM estimates.

Table 2 Correlation of flux tower and DisALEXI ET with ground-based RZSM observations

	March–may		June–september	
	Flux tower	DisALEXI	Flux tower	DisALEXI
SLM001 profile	***– 0.577***	– 0.350	***0.544***	***0.574***
SLM002 profile	***– 0.469***	***– 0.410***	0.240	0.066
RIP720 C1	– 0.031	0.096	***0.449***	***0.526***
RIP720 C2	– 0.244	– 0.069	– 0.034	0.214
RIP720 C3	– 0.175	0.159	0.316	***0.584***
RIP720 C4	– 0.170	– 0.035	0.056	***0.393***

Bold and italicized values indicate corresponding *p* values below the 0.05 significance level

DisALEXI ET

Comparable evaluation can be performed for DisALEXI ET retrievals. Table 2 examines the temporal correlation between various ET estimates and observed RZSM—and, therefore,prospects for VIDA accurately constraining RZSM through the assimilation of ET retrievals. A strong seasonal contrast is found in all comparisons. Observed ET (both from flux towers and DisALEXI) generally has a negative correlation with RZSM in the spring–which is unsurprising given that ample RZSM and low LAI levels in this period leads to ET being primarily energy-constrained (versus water-limited). This was also found in the multi-year analysis of SLM001 and SLM002 RZSM and tower ET measurements by (Wilson et al. 2020). In such cases, ET is not a reliable proxy for RZSM. However, during the summer, the sign of the observed ET-RZSM correlation is reversed, indicating that vineyard ET is now partially constrained by soil–water availability and DisALEXI ET retrievals generally have a

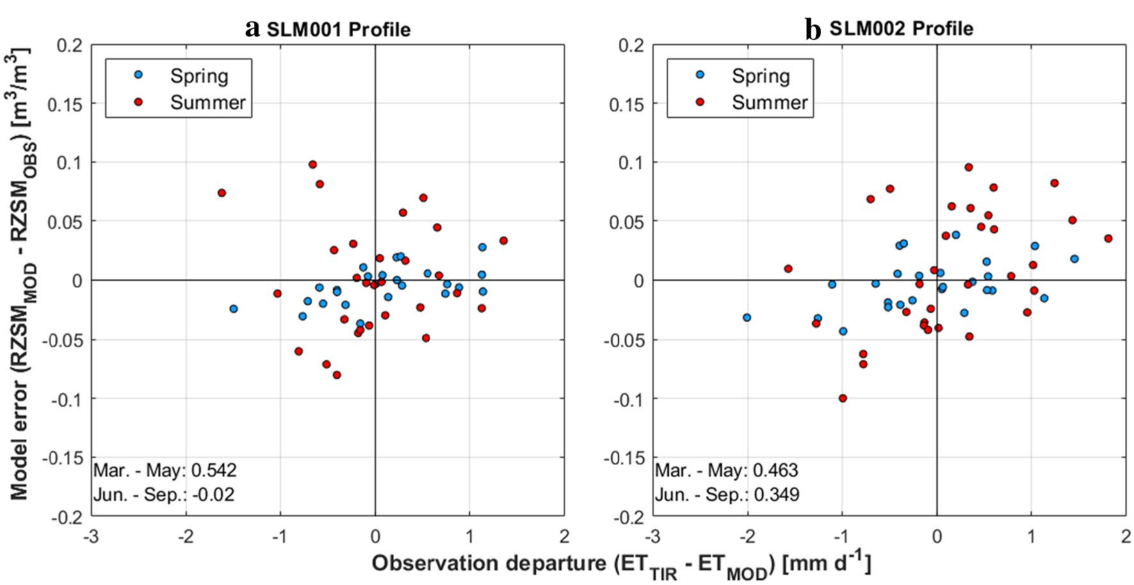

Fig. 6 Pre-assimilation WEB-SVAT RZSM errors (RZSMMOD—RZSMOBS) versus departure between DisALEXI ET and model pre-assimilation ET (ETTIR—ETMOD) at SLM between January 01, 2017 and June 30, 2019. Data points are distinguished by season (spring: March–May, summer: June–September) in (**a**–**b**). Correlations between model error and observation departures are given in the lower left of each subplot

positive coupling with RZSM (see also Wilson et al. 2020). This is consistent with past research that has demonstrated the ability of DisALEXI ET to detect the appearance of water stress (Knipper et al. 2019b). Comparable results are found for flux-tower-based ET in Table 2, demonstrating the relatively good agreement between DisALEXI and eddy covariance ET estimates at these sites.

Paralleling SSM results in Figs. 5, 6 shows the comparison between pre-assimilation WEB-SVAT errors in RZSM (defined as 30–60 cm beneath the vine-row) and observed departures between WEB-SVAT-modelled ET and DisALEXI ET. As discussed above, higher efficiency in assimilating DisALEXI ET is expected during summer than in spring. However, sampled correlations between modelled RZSM errors and observed ET departures in Fig. 6 remain relatively small—even during the summertime. This lack of correlation appears to be tied to irrigation patterns that (basically) maintain water-stress-free conditions during the summer. Studies have shown that grapevines start to show signs of stress at – 50% PAW depletion (Keller 2015; Williams and Trout 2005), making it a useful threshold below which to assume the onset of positive ET-RZSM coupling. However, during our period of study, observed RZSM in SLM rarely drops below 50% PAW (see Figs. 7, 8 below) —thus limiting summertime opportunities for effectively constraining RZSM via the assimilation of ET.

VIDA efficiency and challenges

As described above, the full VIDA system, including the assimilation of remote-sensing observations into the WEB-SVAT model, was run on the SLM001 and SLM002 profile pixels for the period of January 1, 2017 to December 31, 2020. Note that from January 1, 2017 to June 8, 2019, Sentinel-1 SSM and DisALEXI ET retrievals were simultaneously assimilated. Afterwards, only DisALEXI ET was assimilated due to the discontinuation of Sentinel-1 SSM data in early summer 2019. Likewise, VIDA was also run on the RIP720 C1-C4 pixels for the period October 1, 2017 to September 15, 2021 and based on the assimilation of DisALEXI ET retrievals only.

VIDA application to the SLM blocks

As discussed above, pre-assimilation WEB-SVAT profile soil moisture estimates in SLM (Figs. 7, 8) contain

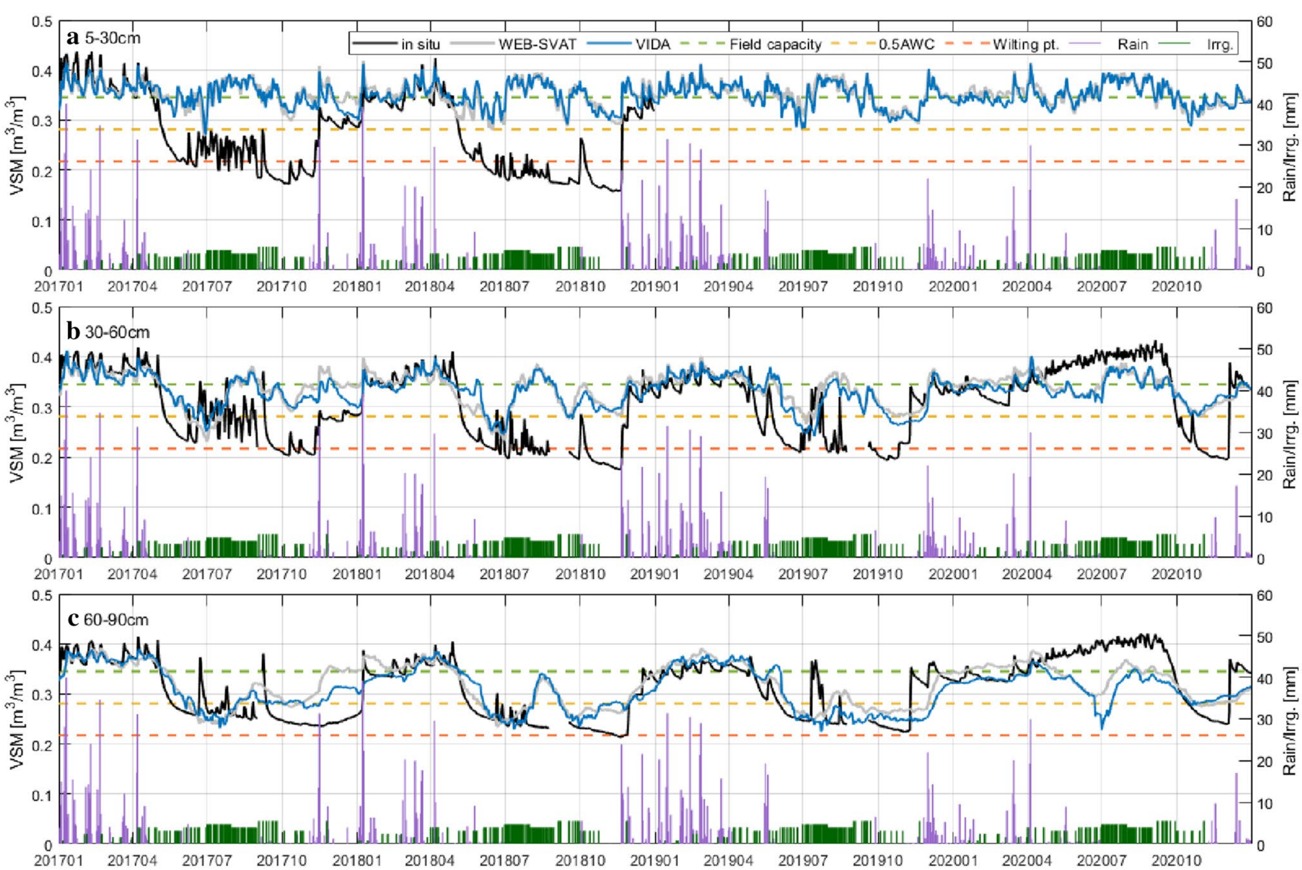

Fig. 7 Modelled (pre-assimilation WEB-SVAT in gray and the EnKF VIDA analysis in blue) and observed vine-row profile soil moisture (dark lines) for the SLM001 profile pixel from January 1, 2017 to December 31, 2020

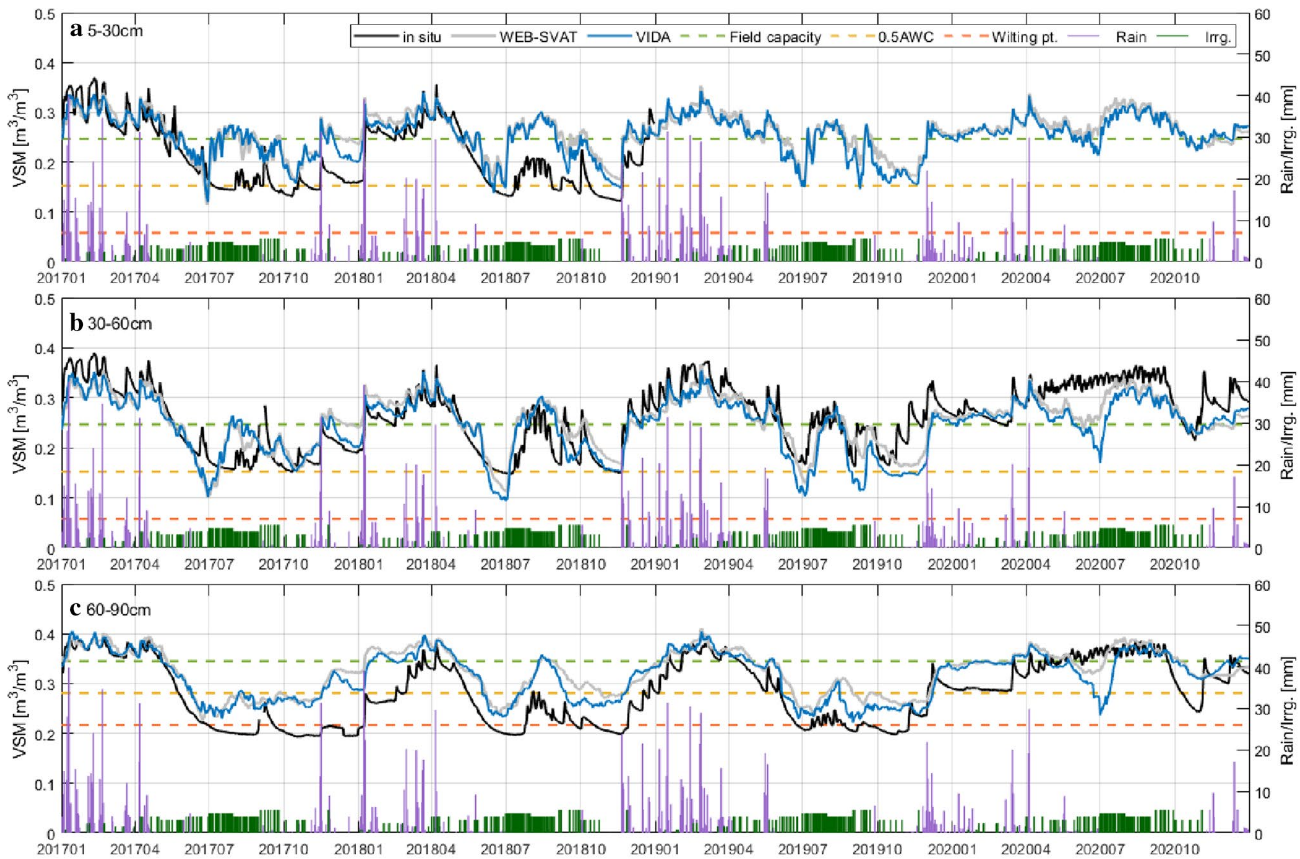

Fig. 8 Same as Fig. 7 but for the SLM002 profile pixel

year-to-year and site-to-site variations in growing-season model bias caused by our use of a fixed irrigation schedule. A key goal here is minimizing these errors using satellite data assimilation. Unfortunately, VIDA displays only limited success in correcting pre-assimilation WEB-SVAT errors. While pre-assimilation WEB-SVAT generally overestimates RZSM in 2017–2019, it severely underestimates RZSM in 2020 when both SLM blocks were grafted to a new grape variety and vigorous irrigation throughout the growing season was applied to ensure new vine growth. Hence, ET in 2020 was limited primarily by the low LAI of the newly grafted vines despite high observed RZSM. Unfortunately, VIDA misinterprets low DisALEXI ET retrivals as water stress caused by low RZSM levels and, as a result, exacerbates the dry bias found in 2020 pre-assimilation WEB-SVAT estimates.

Table 3 summarizes the root-mean-square error (RMSE) and Pearson's correlation metrics of the vine-row 30–60 cm RZSM from (pre-assimilation) WEB-SVAT results and the EnKF-based VIDA analysis. Except for relatively significant improvements during the summer months in the SLM001 pixels, pre-assimilation WEB-SVAT RZSM estimates at SLM during the growing season are generally degraded in VIDA results reflecting the assimilation of satellite retrievals.

These results highlight two major challenges for VIDA. First, a single prescribed irrigation schedule is often incapable of adequately characterizing year-to-year variation in real irrigation practices. Second, data assimilation may result in degraded RZSM estimates when an underlying assumption of positive ET-RZSM coupling does not hold. Potential solutions to these challenges are discussed later in "Discussion and conclusions".

VIDA application to the RIP720 block

Due to the lack of local Sentinel-1 SSM retrievals, only DisALEXI ET is assimilated in the RIP720 block. Nevertheless, somewhat more positive VIDA results, i.e. greater improvement due to data assimilation, are obtained at RIP720 than at SLM001 and SLM002 (Table 3). In particular, VIDA improves the temporal precision of summertime RZSM estimates.

Table 3 Root-mean-square error (RMSE) and correlation (R) between observed and (pre-assimilation WEB-SVAT and VIDA) modelled estimates of vine-row RZSM for both the SLM profile (January 2017–June 2019) and the RIP720 (January 2018–September 2021) pixels

	Year-round				March–may				June–september			
	RMSE [m^3/m^3]		*R*		RMSE [m^3/m^3]		*R*		RMSE [m^3/m^3]		*R*	
	WEB-SVAT	VIDA	WEB-SVAT	VIDA	WEB-SVAT	VIDA	WEB-SVAT	VIDA	WEB-SVAT	VIDA	WEB-SVAT	VIDA
SLM001 profile	0.064	0.062	***0.598***	***0.609***	0.036	0.041	***0.677***	***0.500***	0.083	0.079	***0.343***	***0.377***
SLM002 profile	0.039	0.044	***0.796***	***0.775***	0.026	0.031	***0.760***	***0.698***	0.046	0.058	***0.754***	***0.654***
RIP720 C1	0.044	0.040	***0.646***	***0.714***	0.050	0.046	***− 0.259***	***− 0.143***	0.041	0.037	***0.170***	***0.458***
RIP720 C2	0.066	0.061	***0.713***	***0.750***	0.061	0.054	− 0.003	0.065	0.073	0.070	0.071	***0.372***
RIP720 C3	0.044	0.044	***0.764***	***0.741***	0.049	0.047	***− 0.181***	0.004	0.040	0.033	***0.367***	***0.564***
RIP720 C4	0.045	0.046	***0.680***	***0.703***	0.051	0.054	***− 0.191***	***0.108***	0.042	0.040	***0.221***	***0.464***

Bold and italicized *R* values indicate corresponding *p* values below the 0.05 significance level

Table 4 Correlation of pre-assimilation WEB-SVAT ET and WEB-SVAT RZSM estimates

	March–may	June–september
SLM001 profile	***− 0.575***	− 0.326
SLM002 profile	***− 0.695***	− 0.238
RIP720 C1	− 0.469	0.051
RIP720 C2	− 0.671	0.162
RIP720 C3	− 0.360	0.002
RIP720 C4	− 0.200	0.075

Bold and italicized values indicate corresponding *p* values below the 0.05 significance level

However, other challenges also emerge at RIP720. As discussed in "DisALEXI ET" ET has only modest skill as an RZSM proxy in the spring when ET is energy limited (Fig. 6). However, while observed ET-RZSM coupling increases (i.e., becomes more strongly positive) during the summer (Table 2), WEB-SVAT fails to make the same transition (Table 4). This is problematic because the EnKF underlying VIDA results uses internal WEB-SVAT ET-RZSM coupling estimates as a guide for extrapolating the impact of ET retrievals onto (unobserved) RZSM state estimates. As a result, the weak or negative internal ET-RZSM coupling in WEB-SVAT dampens the magnitude of EnKF RZSM updates in VIDA.

An interesting contrast in data assimilation outcomes is seen between the 2019 and 2021 growing seasons at RIP720–where pre-assimilation WEB-SVAT results overestimate and underestimate observed RZSM, respectively (Fig. 9). Inter-annual variations in winter rainfall are responsible for both the relatively late start of irrigation in 2019 and the relatively early start in 2021. In both years, the neglect of interannual variation in assumed irrigation causes large pre-assimilation WEB-SVAT RZSM biases during the spring and early summer. Early-season irrigation in 2021 also appears to be higher than average, as there is no observed RZSM dry-down transitioning into the vine-only stage (i.e., Stage III). The assimilation of DisALEXI ET in VIDA successfully corrects the dry bias in 2021 but not the corresponding wet bias 2019. This likely reflects the lack of coupling between RZSM and ET during wet conditions—which ensures that VIDA is better suited for correcting a dry RZSM bias than a wet one.

Overview of operational application

As part of a project sponsored by the NASA Water Resources Applied Science Program, the VIDA system was applied operationally during the 2021 growing season for all vineyards within two 100-km^2 domains in the California

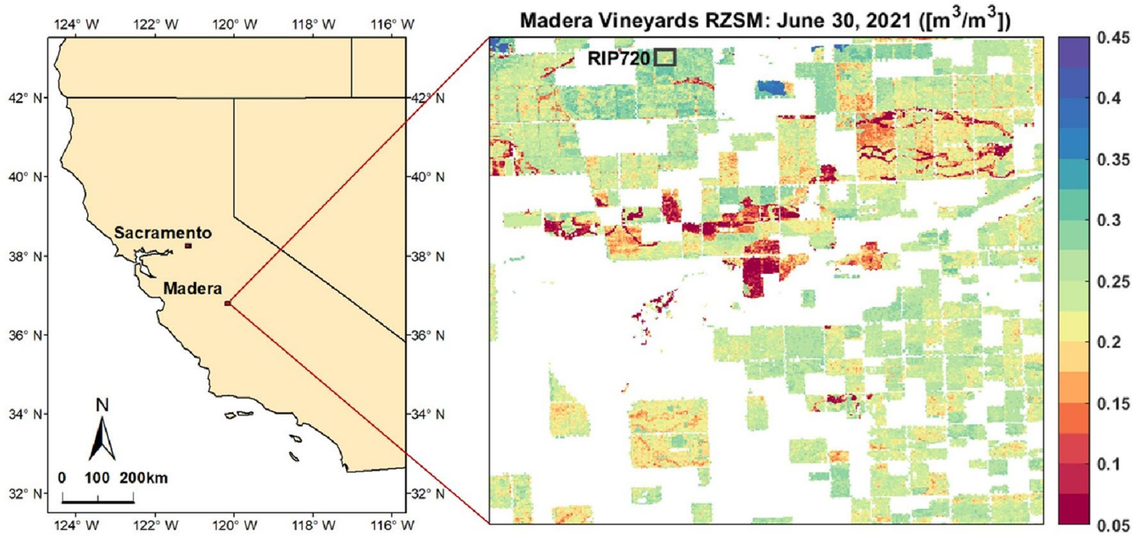

Fig. 9 Location of the Sacramento and Madera 100-km2 operational production vineyard domains in the California Central Valley (left) and an example of an operational VIDA RZSM map on June 30, 2021 for the Madera domain (right). Note that the Madera domain contains the RIP720 block while the Sacramento domain contains the SLM001 and SLM002 blocks discussed above. Results are shown only for areas with vineyard land use

Central Valley (see Fig. 9). Note that the northern "Sacramento" domain (in Sacramento County, CA) includes the SLM001 and SLM002 blocks, and the southern "Madera" domain (in Madera County, CA) includes the RIP720 block. All required VIDA inputs described above in "Meteorological forcing, irrigation inputs, and soil parameters", "Daily LAI and NDVI time-series" can be readily scaled up to cover these larger domains at 30-m resolution. Likewise, assimilated Sentinel-1 SSM and DisALEXI ET retrievals are available operationally (at 2–3 day latency) within both domains. Based on these inputs, the VIDA operational production system generated daily averaged 30-m RZSM (30–60 cm) estimates for each Wednesday during the 2021 growing season (roughly April 1 to September 30). RZSM estimates of vineyards operated by E&J Gallo Winery were then extracted and delivered to Gallo by the following Monday. Figure 9 includes an example of the RZSM imagery generated during the 2021 growing season for the Madera domain.

Discussion and conclusions

While RZSM is commonly recognized as an important variable for the tracking of vineyard water stress, it is seldom directly applied to irrigation decision support. This is largely due to the difficulty of obtaining suitable RZSM estimates. To be of direct value for irrigation decision support, RZSM estimates must be available at: (i) an appropriate vertical soil depth (typically 30 to 60 cm), (ii) a daily time scale, (iii) fine horizontal spatial resolution (likely 30-m in the case of VRDI), and (iv) moderate data latency (likely < 5 days). No single RZSM estimation technique can currently meet all of these requirements. In order to leverage both dynamic water-balance modelling and static satellite remote sensing, the VIDA approach— illustrated retrospectively in "Results and discussion" and then operationally in "Overview of operational application"–is based on the use of a distributed soil water balance model to provide the background for the subsequent sequential updating of soil water profile states using microwave and TIR remote sensing products.

Ignorance concerning the timing and amount of irrigation inputs, both during and after the growing season, represents the primary source of growing-season uncertainty in vineyard RZSM estimates derived from soil water balance modelling (i.e., WEB-SVAT). The VIDA system is based on the hypothesis that, if properly assimilated, microwave-based SSM and TIR-based ET retrievals can be used to reduce random model-based RZSM errors associated with irrigation uncertainty. Therefore, if the VIDA system is to be successfully applied across regional-scale domains (see, e.g., "Overview of operational application"), it must first be robust in the presence of (unknown and inevitable) inter- and intra-annual variations in the application of irrigation.

While there is evidence that the assimilation of both Sentinel-1 SSM retrievals and DisALEXI ET estimates can compensate for dynamic errors present in the WEB-SVAT background (see Figs. 5, 6), the net impact of SSM and ET assimilation on RZSM accuracy is relatively modest and varies widely between sites (Table 3). The lack of uniform improvement associated with the assimilation of Sentinel-1

SSM retrievals and DisALEXI ET can be attributed to a number of unresolved issues.

First, the detection of inter-annual variability in irrigation remains a key challenge. The VIDA system uses random perturbations applied to an assumed irrigation baseline to generate a Monte Carlo ensemble of irrigation realizations that are, in turn, applied to generate a subsequent ensemble of modelled soil water profiles. The EnKF, at the core of the VIDA system, then samples variance and covariance statistics from this ensemble to guide the assimilation of SSM and ET remote sensing retrievals. Our current method for generating this baseline (see "Meteorological forcing, irrigation inputs, and soil parameters") is simplistic and assume that irrigation is a spatially (i.e., within the same geographic domain) and temporally (i.e., year-to-year) stationary process. As a result, it fails to capture inter-annual irrigation variations due to abnormal climate (e.g., anomalous springtime rainfall totals) or shifts in vineyard management (e.g., vine re-grafting). This is problematic because the VIDA EnKF formulation is based on the implicit assumption that the irrigation ensemble is unbiased. As a result, VIDA will fail to update RZSM appropriately in the presence of large inter-annual variability in irrigation applications. This tendency is clearly seen in the RIP720 C3 pixel (Fig. 10) where inter-annual variations in springtime (April–May) irrigation totals cause WEB-SVAT to badly overestimate RZSM in 2019–2020 and underestimate RZSM in 2021. Unfortunately, the subsequent assimilation of Sentinel-1 SSM and DisALEXI ET retrievals leads to only marginal correction of this bias. This suggests the need for more complex background assumptions regarding vineyard irrigation schedules. The development of a more adaptive irrigation baseline, based on field conditions such as weather, vegetation indices, and soil water storage, is currently under investigation.

A second (related) unresolved problem is limitations in the use of remotely sensed ET retrievals as a RZSM proxy. Note that the current VIDA system is based on the use of DisALEXI ET as a diagnostic proxy for RZSM availability and not as a flux estimate (to constrain temporal variations in RZSM). This decision was based on past research showing the ability of DisALEXI ET retrievals to diagnose dynamic water stress in vineyards (Knipper et al. 2019b). However, (Knipper et al. 2019b) also showed that this diagnostic capability is degraded if there is a significant temporal gap or

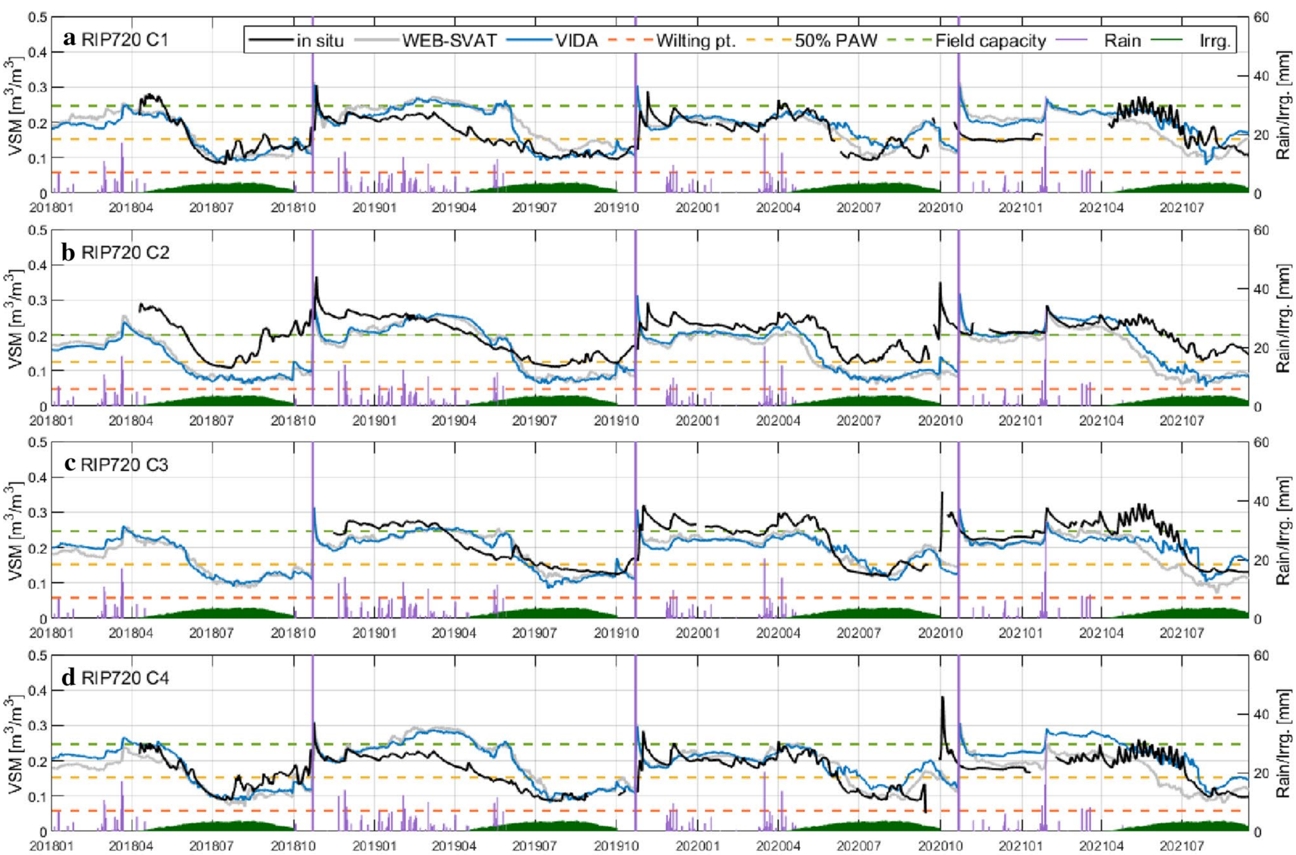

Fig. 10 Modelled and observed vine-yard RZSM (30–60 cm) for the RIP720 C1-C4 pixels between January 1, 2018 and September 15, 2021

delay in acquiring higher resolution Landsat data over the area of interest.

While the quality of DisALEXI vineyard ET retrievals is quite high (Knipper et al. 2019a; 2020), preliminary VIDA results also highlight their limitations as an RZSM proxy. Vine ET varies as a complex function of LAI, canopy radiation loading, micro-meteorological factors, and soil–water availability. The VIDA system relies on the WEB-SVAT model to accurately represent this dependence and define an appropriate RZSM update in response to observed DisALEXI ET variations. However, as noted in "Results and discussion", there are long periods of time where temporal ET dynamics are effectively de-coupled from RZSM and instead reflect changes in canopy LAI and/or micrometeorological conditions. In particular, ET loses sensitivity to RZSM during periods in which it is energy-limited and will therefore struggle to detect cases when irrigation application is significantly underestimated by background WEB-SVAT simulations. These tendencies are clearly seen in the results presented above. For example, VIDA is unable to correct the dry bias in springtime RZSM seen in the RIP720 C2 pixel during 2020 (see Fig. 10). Likewise, VIDA can misattribute reductions in ET to RZSM limitations that in reality are caused by relatively low LAI conditions. This can cause a spurious decrease in VIDA RZSM results—as observed in SLM001 and SLM002 during the 2020 growing season (see Figs. 7, 8). Another potential issue with DisALEXI ET is its inability to quickly respond to the onset of irrigation in the springtime, as the availability of its 30-m component (i.e., LST), nominally anchored by an 8-day Landsat overpass interval, is often even less frequent due to the decreased number of clear data acquisition days.

A final danger is that, even in cases where coupling between RZSM and ET is present, it will not be accurately captured by WEB-SVAT. This is problematic since VIDA relies on WEB-SVAT to capture the relationship between unobserved fluxes (e.g., ET) and unobserved model states (e.g., RZSM). As seen in "DisALEXI ET", "VIDA application to the RIP720 block" when the observed ET-RZSM relationship transitions into a positive correlation during the summer (from the negative correlation in the spring), WEB-SVAT still consistently underestimates the true level of ET-RZSM coupling (compare Tables 2, 4). In such cases, VIDA will squander the value of observed ET as a RZSM constraint.

Comparable limitations also exist for Sentinel-1 SSM retrievals. In particular, during the middle portion of the growing season, their accuracy is degraded by dense vine-canopy coverage. In addition, the shallow vertical support (<5 cm) of SAR-based SSM retrievals makes it difficult for them to detect drip irrigation—which, by design, leaves a wetting pattern over a relatively small fraction of a vineyard's soil surface.

Finally, the use of a simplified 1-D soil water balance model may introduce errors into estimated RZSM levels. Within VIDA, the horizontal flux of soil water between row and interrow tiles is neglected due to the required complexity and computational cost of 3-D modeling, which makes it difficult to scale the approach up to larger domains, and the relative lack of topographic variability within Central Valley vineyards. However, Fig. 4 suggests that, even for relatively flat vineyards, the neglect of lateral soil–water movement may introduce error in some scenarios such as over-irrigation, when water applied exceeds the infiltration capacity of the upper layers, leading to horizontal flow into the interrow.

Despite the scale of these challenges, notable opportunities exist for improving the extraction of vineyard irrigation information from remote sensing observations. Based on our preliminary results, it appears necessary to consider the value of DisALEXI ET observations as both a RZSM diagnostic proxy and a prognostic indicator of RZSM loss rates. Such dual flux/state approaches have been applied previously in other land data assimilation systems (Chen et al. 2014) and may be of value here. Furthermore, L-band SSM retrievals available from the upcoming NASA-ISRO Synthetic Aperture Radar (NISAR) mission (expected by 2023) should improve upon the (C-band) Sentinel-1 SSM retrievals currently applied in VIDA. In particular, NISAR's L-band capability should improve our ability to resolve SSM under dense vine cover and increase the vertical support of SSM retrievals within the soil column. Likewise, improvements in the temporal responsiveness of TIR-based ET observations have been achieved by augmenting the HLS dataset with Sentinel-2-sharpened VIIRS (Visible Infrared Imaging Radiometer Suite) as a thermal proxy source, thus achieving a potential combined frequency of 2–3 days (Xue et al. 2021). Moreover, a spectral-based ET approach using Sentinel-2 data recently evaluated over vineyards could also improve the frequency of ET retrieval (D'Urso et al. 2021). Finally, new opportunities also exist for using remote sensing observations to critique, and improve upon, the representation of ET versus RZSM coupling in land surface models such as WEB-SVAT (Dong et al. 2020). Future research will prioritize these possibilities to improve upon preliminary VIDA RZSM assimilation results presented here.

Acknowledgements We would like to thank E.J. Gallo Winery and the staff of the Winegrowing Research and Gallo Vineyards for access to vineyard sites, support for deployment of towers and sensors, and assistance in the collection of data used in this study. Financial support for this research was provided by USDA Agricultural Research Service and by grants from NASA Applied Sciences-Water Resources Program Award NNH17AE39I, PI W. Kustas, and 80NSSC19K1245 PI W. Crow). USDA is an equal opportunity provider and employer.

Funding This research is funded by NASA Applied Science Award 80NSSC19K1247 entitled: "High-Resolution Soil Moisture Monitoring for Improved Vineyard Water Resource Management" (PI: W.T. Crow).

Declarations

Conflict of interest On behalf of all authors, the corresponding author states that there is no conflict of interest.

References

Acevedo-Opazo C, Ortega-Farias S, Fuentes S (2010) Effects of grapevine (*Vitis vinifera* L.) water status on water consumption, vegetative growth and grape quality: an irrigation scheduling application to achieve regulated deficit irrigation. Agr Water Manag 97(7):956–964

Agam N, Kustas WP, Alfieri JG, Gao F, McKee L, Prueger JH, Hipps LE (2019) Micro-scale spatial variability in soil heat flux (SHF) in a wine-grape vineyard. Irrig Sci 37:253–268. https://doi.org/10.1007/s00271-019-00634-6

Al Bitar A, Mialon A, Kerr YH, Cabot F, Richaume P, Jacquette E, Quesney A, Mahmoodi A, Tarot S, Parrens M, Al-Yaari A, Pellarin T, Rodriguez-Fernandez N, Wigneron JP (2017) The global SMOS level 3 daily soil moisture and brightness temperature maps. Earth Syst Sci Data 9:293–315. https://doi.org/10.5194/essd-9-293-2017

Alfieri JG, Kustas WP, Prueger JH, McKee L, Hipps LE, Gao F (2019) A multi-year intercomparison of micrometeorological observations at adjacent vineyards in California's Central Valley during GRAPEX. Irrig Sci 37:345–357. https://doi.org/10.1007/s00271-018-0599-3

Anderson MC, Norman JM, Diak GR, Kustas WP, Mecikalski JR (1997) A two-source time integrated model for estimating surface fluxes using thermal infrared remote sensing. Remote Sens Env 60:195–216

Anderson MC, Norman JM, Mecikalski JR, Torn RD, Kustas WP, Basara JB (2004) A multiscale remote sensing model for disaggregating regional fluxes to micrometeorological scales. J Hydrometeorol 5:343–363

Attarzadeh R, Amini J, Notarnicola C, Greifeneder F (2018) Synergetic use of sentinel-1 and sentinel-2 data for soil moisture mapping at plot scale. Remote Sens 10(8):1285. https://doi.org/10.3390/rs10081285

Cammalleri C, Anderson MC, Kustas WP (2014) Upscaling of evapotranspiration fluxes from instantaneous to daytime scales for thermal remote sensing applications. Hydrol Earth Syst Sci 18:1885–1894

Campbell GS, Norman JM (1998) An introduction to environmental geophysics. Springer-Verlag, New York, p 286

Chan SK, Bindlish R, O'Neill P et al (2018) Development and assessment of the SMAP enhanced passive soil moisture product. Remote Sens Env 204:931–941. https://doi.org/10.1016/j.rse.2017.08.025

Chen F, Crow WT, Ryu D (2014) Dual forcing and state correction via soil moisture assimilation for improved rainfall-runoff modeling. J Hydrometeor 15(5):1832–1848. https://doi.org/10.1175/JHM-D-14-0002.1

Clapp RB, Hornberger GM (1978) Empirical equations for some soil hydraulic properties. Water Resour Res 14(4):601–604

Claverie M, Ju J, Masek JG, Dungan JL, Vermote EF, Roger JC, Skakun SV, Justice C (2018) The harmonized landsat and sentinel-2 surface reflectance data set. Remote Sens Env 219:145–161. https://doi.org/10.1016/j.rse.2018.09.002

Crow WT, Kustas WP, Prueger J (2008) Monitoring root-zone soil moisture through the assimilation of a thermal remote sensing-based soil moisture proxy into a water balance model. Remote Sens Env 112:1268–1281

D'Urso G, Bolognesi SF, Kustas WP, Knipper KR, Anderson MC, Alsina MM, Hain CR, Alfieri JG, Prueger JH, Gao F, McKee L, Michele CD, McElrone AJ, Bambach NE, Sanchez L, Belfiore OR (2021) Determining evapotranspiration by using combination equation models with sentinel-2 data and comparison with thermal-based energy balance in a California irrigated vineyard. Remote Sens 13:3720

Das N, Entekhabi D, Dunbar S, Chaubell J, Colliander A, Yueh S, Jagdhuber T, Chen F, Crow WT, O'Neill PE, Walker J, Berg A, Bosch D, Caldwell T, Cosh M, Collins CH, Lopez-Baeza E, Thibeault M (2019) The SMAP and copernicus sentinel 1A/B microwave active-passive high resolution surface soil moisture product. Remote Sens Env 233:111380. https://doi.org/10.1016/j.rse.2019.111380

Diffenbaugh NS, Swain DL, Touma D (2015) Anthropogenic warming has increased drought risk in California. Proc of the Natl Acad Sci 112(13):3931–3936. https://doi.org/10.1073/pnas.1422385112

Dong J, Dirmeyer PA, Lei F, Anderson MC, Holmes TRH, Hain C, Crow WT (2020) Soil evaporation stress determines soil moisture-evapotranspiration coupling strength in land surface modeling. Geophys Res Lett. https://doi.org/10.1029/2020GL090391

El Hajj M, Baghdadi N, Zribi M, Bazzi H (2017) Synergic use of sentinel-1 and sentinel-2 images for operational soil moisture mapping at high spatial resolution over agricultural areas. Remote Sens 9(12):1292. https://doi.org/10.3390/rs9121292

Gao F, Anderson MC, Kustas WP, Wang Y (2012a) Simple method for retrieving leaf area index from Landsat using MODIS leaf area index products as reference. J Appl Remote Sens 6(1):063554. https://doi.org/10.1117/1.JRS.6.063554

Gao F, Kustas WP, Anderson MC (2012b) A data mining approach for sharpening thermal satellite imagery over land. Remote Sens 4:3287–3319

Gao F, Anderson MC, Kustas WP, Houborg R (2013) Retrieving leaf area index from Landsat using MODIS LAI products and field measurements. IEEE Geosci Remote Sens Lett 11:773–777. https://doi.org/10.1109/LGRS.2013.2278782

Gao Q, Zribi M, Escorihuela M, Baghdadi N (2017) Synergetic use of sentinel-1 and sentinel-2 data for soil moisture mapping at 100 m resolution. Sensors 17(9):1966. https://doi.org/10.3390/s17091966

Gao F, Anderson MC, Daughtry CS, Karnieli A, Hively WD, Kustas WP (2020) A within-season approach for detecting early growth stages in corn and soybean using high temporal and spatial resolution imagery. Remote Sens Env 242:111752. https://doi.org/10.1016/j.rse.2020.111752

Gerhards M, Schlerf M, Mallick K, Udelhoven T (2019) Challenges and future perspectives of multi-/hyperspectral thermal infrared remote sensing for crop water-stress detection: a review. Remote Sens 11(10):1240. https://doi.org/10.3390/rs11101240

Gish TJ, Walthall CL, Daughtry CS, Kung KJ (2005) Using soil moisture and spatial yield patterns to identify subsurface flow pathways. J Env Qual 34(1):274–286. https://doi.org/10.2134/jeq2005.0274

Greifeneder F, Notarnicola C, Wagner WA (2021) Machine learning-based approach for surface soil moisture estimations with google earth engine. Remote Sens 13:2099. https://doi.org/10.3390/rs13112099

Hain CR, Mecikalski JR, Anderson MC (2009) Retrieval of an available water-based soil moisture proxy from thermal infrared remote sensing part I: methodology and validation. J Hydrometeorol 10:665–683. https://doi.org/10.1175/2008JHM1024.1

Hashemian M, Ryu D, Crow WT, Kustas WP (2015) Improving root-zone soil moisture estimations using dynamic root growth and crop phenology. Adv Water Resour 86:170–183

Huning LS, AghaKouchak A (2018) Mountain snowpack response to different levels of warming. Proc Natl Acad Sci 115(43):10932–10937

Hupet F, Vanclooster M (2002) Interseasonal dynamics of soil moisture variability within a small agricultural maize cropped field. J Hydrol 261:86–101. https://doi.org/10.1016/S0022-1694(02)00016-1

Jasechko S, Perrone D (2020) California's Central Valley groundwater wells run dry during recent drought. Earth's Future. https://doi.org/10.1029/2019EF001339

Keller M (2015) The science of grapevines: anatomy and physiology, 2nd edn. Academic Press, Elsevier, London

Keller M, Romero P, Gohil H, Smithyman RP, Riley WR, Casassa LF, Harbertson JF (2016) Deficit irrigation alters grapevine growth, physiology, and fruit microclimate. Am J Enol Vitic 67:426–435. https://doi.org/10.5344/ajev.2016.16032

Knipper KR, Kustas WP, Anderson MC, Alfieri JG, Prueger JH, Hain CR, Gao F, Yang Y, McKee L, Nieto H, Hipps LE, Alsina MM, Sanchez LA (2019a) Evapotranspiration estimates derived using thermal-based satellite remote sensing and data fusion for irrigation management in California vineyards. Irrig Sci 37:431–449. https://doi.org/10.1007/s00271-018-0591-y

Knipper KR, Kustas WP, Anderson MC, Alsina MM, Hain CR, Alfieri JG, Prueger JH, Gao F, McKee LG, Sanchez LA (2019b) Using high-spatiotemporal thermal satellite ET retrievals for operational water use and stress monitoring in a California vineyard. Remote Sens 11(18):2124. https://doi.org/10.3390/rs11182124

Knipper KR, Kustas WP, Anderson M, Nieto H, Alfieri JG, Prueger JH, Hain CR, Gao F, McKee L, Alsina MM, Sanchez L (2020) Using high-spatiotemporal thermal satellite ET retrievals to monitor water use over California vineyards of different climate, vine variety and trellis design. Agr Water Manag. https://doi.org/10.1016/j.agwat.2020.106361

Kukal MS, Irmak S (2019) Irrigation-limited yield gaps: trends and variability in the United States post-1950. Env Res Commun 1:061005

Kustas WP, Anderson MC, Alfieri JG, Knipper K, Torres-Rua A, Parry CK, Nieto H, Agam N, White WA, Gao F, McKee L, Prueger JH, Hipps LE, Los S, Alsina MM, Sanchez L, Sams B, Dokoozlian N, McKee M, Jones S, Yang Y, Wilson TG, Lei F, McElrone A, Heitman JL, Howard AM, Post K, Melton F, Hain C (2018) The grape remote sensing atmospheric profile and evapotranspiration experiment. Bull Am Meteorol Soc 99(9):1791–1812. https://doi.org/10.1175/bams-d-16-0244.1

Lei F, Crow WT, Kustas WP, Dong J, Yang Y, Knipper KR, Anderson MC, Gao F, Notarnicola C, Greifeneder F, McKee LM, Alfieri JG, Hain C, Dokoozlian N (2020) Data assimilation of high-resolution thermal and radar remote sensing retrievals for soil moisture monitoring in a drip-irrigated vineyard. Remote Sens Env. https://doi.org/10.1016/j.rse.2019.111622

Li KY, De Jong R, Boisvert JB (2001) An exponential root-water-uptake model with water stress compensation. J Hydrol 252(1–4):189–204

Li F, Kustas WP, Anderson MC, Prueger JH, Scott RL (2008) Effect of remote sensing spatial resolution on interpreting tower-based flux observations. Remote Sens Env 112:337–349. https://doi.org/10.1016/j.rse.2006.11.032

Montaldo N, Albertson JD, Marcini M, Kiely G (2001) Robust prediction of root zone soil moisture from assimilation of surface soil moisture. Water Resour Res 37:2889–2900

Myneni R, Hoffman S, Knyazikhin Y, Privette J, Glassy J, Tian Y, Wang Y, Song X, Zhang Y, Smith G, Lotsch A, Friedl M, Morisette J, Votava P, Nemani R, Running S (2002) Global products of vegetation leaf area and fraction absorbed PAR from year one of MODIS data. Remote Sens Env 83:214–231. https://doi.org/10.1016/S0034-4257(02)00074-3

Naeimi V, Scipal K, Bartalis Z, Hasenauer S, Wagner W (2009) An improved soil moisture retrieval algorithm for ERS and MetOp scatterometer observations. IEEE Trans Geosci Remote Sens 47(7):1999–2013. https://doi.org/10.1109/TGRS.2008.2011617

Nieto H, Kustas WP, Torres-Rúa A, Alfieri JG, Gao F, Anderson MC et al (2019) Evaluation of TSEB turbulent fluxes using different methods for the retrieval of soil and canopy component temperatures from UAV thermal and multispectral imagery. Irrig Sci 37(3):389–406. https://doi.org/10.1007/s00271-018-0585-9

Noilhan J, Planton S (1989) A simple parameterization of land surface processes in meteorologic models. Mon Weather Rev 117:536–549

Noorduijn SL, Hayashi M, Mohammed GA, Mohammed AA (2018) A coupled soil water balance model for simulating depression-focused groundwater recharge. Vadose Zone J 17(1–14):170176. https://doi.org/10.2136/vzj2017.10.0176

Norman JM, Kustas WP, Humes KS (1995) Source approach for estimating soil and vegetation energy fluxes in observations of directional radiometric surface temperature. Agr for Meteorol 77(3–4):263–293. https://doi.org/10.1016/0168-1923(95)02265-Y

Norman JM, Anderson MC, Kustas WP, French AN, Mecikalski J, Torn R, Diak GR, Schmugge TJ, Tanner BCW (2003) Remote sensing of surface energy fluxes at 101-m pixel resolutions. Water Resour Res 39:1221

Oh Y (2004) Quantitative retrieval of soil moisture content and surface roughness from multipolarized radar observations of bare soilsurfaces. IEEE Trans Geosci Remote Sens 42:596–601

Sanchez LA, Sams B, Alsina MM, Hinds N, Klein LJ, Dokoozlian N (2017) Improving vineyard water use efficiency and yield with variable rate irrigation in California. Adv Anim Biosci 8(2):574–577. https://doi.org/10.1017/S2040470017000772

Sellers PJ, Heiser MD, Hall FG (1992) Relations between surface conductance and spectral vegetation indices at intermediate (100 m^2–15 km^2) length scales. J Geophys Res 97:19033–19059

Semmens K, Anderson MC, Kustas WP, Gao F, Alfieri JG, McKee L, Prueger JH, Hain CR, Cammalleri C, Yang Y, Xia T, Sanchez LA, Alsina MM, Vélez M (2016) Monitoring daily evapotranspiration over two California vineyards using landsat 8 in a multi-sensor data fusion approach. Remote Sens Env 185:155–170. https://doi.org/10.1016/j.rse.2015.10.025

Shellie KC (2014) Water productivity, yield, and berry composition in sustained versus regulated deficit irrigation of Merlot grapevines. Am J Enol Vitic 65:197–205. https://doi.org/10.5344/ajev.2014.13112

Sun L, Gao F, Anderson M, Kustas WP, Alsina M, Sanchez L, Brent S, McKee LG, Dulaney WP, White A, Alfieri JG, Prueger JH, Melton F, Post K (2017) Daily mapping of 30m LAI and NDVI for grape yield prediction in California vineyards. Remote Sens 9:317. https://doi.org/10.3390/rs9040317

Verdoodt A, Ranst EV, Ye L, Verplancke H (2005) A daily multi-layered water balance model to predict water and oxygen availability in tropical cropping systems. Soil Use Manag 21:312–321

White WA, Alsina MM, Nieto H, McKee LG, Gao F, Kustas WP (2019) Determining a robust indirect measurement of leaf area index in California vineyards for validating remote sensing-based retrievals. Irrig Sci 37:269–280. https://doi.org/10.1007/s00271-018-0614-8

Williams LE, Trout TJ (2005) Relationships among vine- and soil-based measures of water status in a thompson seedless vineyard in response to high frequency drip irrigation. Am J Enol Vitic 56:357–366

Wilson TG, Kustas WP, Alfieri JG, Anderson MC, Gao F, Prueger JH, McKee L, Alsina MM, Sanchez LA, Alstad KP (2020) Relationships between soil water content, evapotranspiration, and irrigation measurements in a California drip-irrigated pinot noir vineyard. Agr Water Manag 237:106186. https://doi.org/10.1016/j.agwat.2020.106186

Xia Y, Mitchell K, Ek M, Sheffield J, Cosgrove B, Wood E, Luo L, Alonge C, Wei H, Meng J, Livneh B, Lettenmaier D, Koren V, Duan Q, Mo K, Fan Y, Mocko D (2012) Continental-scale water and energy flux analysis andvalidation for the North American Land Data assimilation system project phase 2 (NLDAS-2): 1. Intercomparisonand application of model products. J Geophys Res 117:D03109. https://doi.org/10.1029/2011JD016048

Xue J, Anderson MC, Gao F, Knipper K, Hain C, Yang Y, Yang Y (2021) Mapping daily evapotranspiration at field scale using the harmonized landsat/sentinel-2 (HLS) dataset, with sharpened VIIRS as a sentinel-2 thermal proxy. Remote Sens 13(17):3420. https://doi.org/10.3390/rs13173420

Yan K, Park T, Yan G, Chen C, Yang B, Liu Z, Nemani RR, Knyazikhin Y, Myneni RB (2016) Evaluation of MODIS LAI/FPAR product collection 6 part 1: consistency and improvements. Remote Sens 8(5):359. https://doi.org/10.3390/rs8050359

Zarrouka O, Francisco R, Pinto-Marijuan M, Brossa R, Santos RR, Pinheiro C, Costa JM, Lopes C, Chaves MM (2012) Impact of irrigation regime on berry development and flavonoids composition in Aragonez (Syn. Tempranillo) grapevine. Agr Water Manag 114:18–29